Caloxin-derived peptides for the inhibition of plasma membrane calcium ATPases

Jean Boutin, Stéphane Bedut, Magali Jullian, Mathieu Galibert, Lukasz Frankiewicz, Philippe Gloanec, Gilles Ferry, Karine Puget, Jérôme Leprince

Caloxin-derived peptides for the inhibition of plasma membrane calcium ATPases

Jean A. Boutin[1,2], Stéphane Bedut[4], Magali Jullian[3], Mathieu Galibert[3], Lukasz Frankiewicz[3,¤], Philippe Gloanec[5], Gilles Ferry[1], Karine Puget[3], Jérôme Leprince[2,6]

[1] Institut de Recherches Servier, Croissy-sur-Seine, France
[2] INSERM U1239, University of Rouen Normandy, Laboratory of Neuroendocrine Endocrine and Germinal Differentiation and Communication (NorDiC), Rouen, France
[3] Genepep SAS, Saint Jean de Vedas, France
[4] E-Physervices, Paris, France
[5] Institut de Recherches Servier, Suresnes, France
[6] INSERM US51, University of Rouen Normandy, Cell Imaging Platform of Normandy (PRIMACEN), Rouen, France
[¤] present address: Gyros Protein Technologies AB, Uppsala, Sweden

Corresponding author: Jean A. Boutin, ja.boutin.pro@gmail.com

Abstract: Plasma membrane calcium ATPases (PMCAs) are a family of transmembrane proteins responsible for the extrusion of cytosolic Ca^{2+} to the extracellular milieu. They are important players of the calcium homeostasis possibly implicated in some important diseases. The reference inhibitors of PMCA extruding activity are on one hand ortho-vanadate (IC_{50} in the 30 mM range), and on the other a series of 12- to 20-mer peptides named caloxins (IC_{50} in the 100 µM scale). As for all integral membrane proteins, biochemistry and pharmacology are difficult to study on isolated and/or purified proteins. Using a series of reference blockers, we assessed a pharmacological window with which we could study the functionality of PMCAs in living cells. Using this system, we screened for alternative versions of caloxins, aiming at shortening the peptide backbone, introducing non-natural amino acids, and overall trying to get a glimpse at the structure-activity relationship between those new peptides and the protein in a cellular context. We describe a short series of equipotent 5-residue long analogues with IC_{50} in the low µM range.

Keywords: PMCA; peptide inhibitor; caloxins; calcium efflux; cellular test.

1. Introduction

Plasma membrane calcium ATPases (PMCAs) are key components of the cellular calcium homeostasis [1]. They form a family of four-member family of transmembrane proteins that actively transports calcium throughout the plasma membrane in a highly regulated manner in non-excitable cells [1,2]. They correspond to ATP-driven Ca^{2+} pumps largely expressed in eukaryotic cells and their role is mainly to maintain a low resting cytosolic concentration of calcium. These integral membrane proteins exist in many different isoforms resulting from differential splicing for which individual roles are still largely missing. They are involved in a wide range of pathological conditions in animal models and human diseases [3]. Recent advances strongly suggest that PMCAs might have a role in surviving of cancer cells [4], particularly in pancreas cancer cells [5]. Therefore, new actors in the pharmacology of these transporters could present interesting new clinical routes towards anticancer therapies.

Methodologies to isolate and address PMCA function have essentially relied on their purification and reconstitution in artificial vesicles [6], and often focused on the detection of the ATPase activity of the pump rather than on the calcium fluxes themselves. For the sake of screening purposes, we reasoned that PMCA function could be specifically addressed in living cells (*i*) by using calcium movements as readout and (*ii*) by designing a "functional isolation" approach instead of using the classical "physical isolation" strategy where the pump works in a completely artificial environment. Indeed, in a living cell, cytosolic calcium concentration at each time point is a snapshot of the dynamic equilibrium established between the activity of the different Ca^{2+} channels/pumps bringing calcium to the cytosol and the concomitant reverse activity of channels and pumps by extrusion to the extracellular space and/or by sequestration into subcellular organelles leading to the global cellular calcium homeostasis (**Scheme 1A**). Pumps removing calcium are particularly active when calcium concentration is high during which time, they take a net lead over the calcium influx mechanisms. Using the available well characterized inhibitors of the contributors of the calcium homeostasis, we defined a combination of pharmacological blockers capable to functionally trigger a net cytosolic calcium clearance condition (*i.e.* "window") exclusively supported by the PMCA function. This pharmacological window can be easily studied by kinetic fluorescence 96-well plate imaging of living

cultured cells. For this purpose, we used HEK 293 cells in which PMCA4 is the main native PMCA isoform expressed [4,7].

Since the concentration of one of the main reference PMCA inhibitors, ortho-vanadate (oVa), used in the cellular assays is very high (in the 30 mM range) and its specificity towards other cellular systems not guaranteed, several possibilities were previously explored to find alternative reference compounds inhibiting PMCAs such as lanthanum salts [8] or carboxyeosine [9]. Lanthanum salts tend to precipitate with many different anions from µM concentrations and inhibit PMCA at mM concentrations, while the use of carboxyeosin is hampered by its membrane impermeability (see Chen et al for discussion [10]. In addition, the group of Grover found by different means several 20-amino-acid long peptides, named caloxins, with interesting inhibitory capacities on these particular proteins [11]. Nevertheless, these peptides were not optimized and thus, the field still suffers of a lack of more easily attainable and trustable tools.

In the present study, we designed an assay for PMCA inhibition using HEK 293 cells [7]. Our understanding is that HEK 293 cells express mainly PMCA4 with traces of PMCA1, leading to the possibility that even small amount of PMCA1 could interfere with the whole process. The goal was to discover potent inhibitors of PMCA-dependent calcium movements in living cells in a screening-friendly 96 wells plate format. We used a FLIPR^{TETRA} in a high-throughput assay mode (as opposed to high-throughput screening format). This automatic instrument insured the repetitivity of the assays within a 96-weel plate format. The instrument has been previously described for intracellular Ca^{2+} measurement by the manufacturer [12] and by several laboratories [13,14], including ours, in the characterization of newly discovered receptor functionality [15]. We used all the reported caloxins as starting materials [16–19] with the aim of simplifying the sequence as a first step, particularly by shortening these peptides. Their use in an initial step of our assay also validated the assay, as comforting results were obtained, in comparison to the original data obtained with a completely different assay [20]. More than one hundred of analogues were synthesized, characterized, and tested. The final peptides we described are more potent than the parent peptides and potentially more specific than the reference PMCA inhibitor, oVa. Incidentally, the present work is among the first ones

screening for finding PMCA inhibitors by measuring its calcium trafficking, as opposed to the often use of PMCA ATPase activity measurement in most of the research for PMCA inhibitor/antagonist [21–23].

2. Materials and Methods

2.1 Reagents: Standard Fmoc-amino acids and D-counterparts, Oxyma Pure, *N,N'*-diisopropylcarbodiimide (DIC), Fmoc-Rink-amide aminomethyl-polystyrene resin, and preloaded Fmoc-Gly-2-chlorotrityl resin and Fmoc-Arg(Pbf)-Wang resin were purchased from Iris Biotech (Marktredwitz, Germany). Boc-Lys(Fmoc)-OH and other non-standard Fmoc-amino-acid building blocks are from Sigma-Aldrich (Saint-Quentin-Fallavier, France), Iris Biotech, Eurogentec (Seraing, Belgium), ACROS (Illkirch-Graffenstaden, France), Eurogentec (Seraing, Belgique), Bachem (Bubendorf, Switzerland) or custom-synthesized for Servier Laboratories. Acetic anhydride, acetonitrile (HPLC grade), ascorbic acid, dimethylformamide (DMF), dimethylsulfoxide (DMSO), dichloromethane (DCM), hexafluoroisopropanol (HFIP), I_2, methanol, diethylether, trifluoroacetic acid (TFA), piperidine and triisopropyl silane (TIS) were supplied from Sigma-Aldrich.

2.2 Peptide synthesis: All peptides were synthesized by Fmoc solid phase methodology on a SymphonyX instrument (Gyros Protein Technologies AB, Uppsala, Sweden) using the standard manufacturer's procedures at 100 µmol scale. Briefly, The standard deprotection-coupling cycle for each residue consists of six steps: (*i*) Wash of the resin with 5 mL of DMF (3 x 30 sec); (*ii*) On-resin Fmoc group deprotection with 5 mL of 20% piperidine in DMF (3 x 3 min); (*iii*) Wash of the resin with 5 mL of DMF (3 x 30 sec); (*iv*) Fmoc-AA-OH coupling (2 x 60 min), a) 5 mL of 0.2 M (10 eq.) Fmoc-AA-OH in DMF, b) 2 mL of 0.5 M (10 eq.) Oxyma Pure in DMF, and c) 1 mL of 1 M (10 eq.) DIC in DMF; (*v*) Capping with 5 mL of 10% Ac_2O in DMF (7 min) and finally (*vi*) Wash with 5 mL of DMF (3 x 30 sec). After completion of the chain assembly, peptidyl resins were washed thrice with DCM. Peptides were deprotected and cleaved from the resin by adding 10 mL of cleavage cocktail TFA/TIS/H_2O (90:5:5). for 180 min at room temperature. Cleavage solution was filtered from the resin and peptides were precipitated by addition to 40 mL of ice-cold diethylether. After >1 h at -20 °C, ethered layer was centrifuged at 3500 RCF and the supernatant was decanted. Pellets were washed twice with diethylether and then dried for >3 h in a vacuum desiccator prior to dissolution for analytical characterization and purification. The peptides were analyzed by UPLC at 214 nm on a 150 × 2.1 mm BEH C_{18} column (Waters, Guyancourt, France) using a linear gradient of acetonitrile/TFA (99.9:0.1) at a flow rate of 0.6 mL/min and by ESI mass spectrometry.

2.3 Cal1b332 head-to-tail cyclic peptide synthesis: The linear precursor of **cal1b332** was synthesized on a preloaded Fmoc-Gly-2-chlorotrityl resin as described above. After completion of the chain assembly, the linear peptide was released from the resin as a fully sidechain protected peptide by adding 20 mL of the mixture HFIP/DCM (2:8, 3 × 30 min, room temperature). The combined organic layers were concentrated under reduced pressure to obtain crude peptide. The linear protected peptide was then dissolved in DCM (1 mM) and 2 eq. of Oxyma Pure and 2 eq. of DIC were added. Reaction mixture was stirred overnight at room temperature for lactamization. Solvent was removed under

reduced pressure and the crude head-to-tail cyclic peptide was side-chain deprotected and characterized as described above.

2.4 Disulfide bridge formation: Crude sulfhydryl peptides were dissolved (1 mM) in H_2O/TFA (99.9:0.1) and a 60 mM solution of iodine in MeOH was added dropwise with rapid stirring until the solution had a slight yellow color. Iodine excess was quenched with 1 M ascorbic acid prior to analytical characterization as described above.

2.5 Peptide purification: Crude peptides were purified by reversed-phase HPLC with a Delta Prep 4000 system (Waters) on a 50 × 300 mm Vydac Denali prep C-18 (10 µm, 120 Å) column using an appropriate gradient of acetonitrile/TFA (99.9:0.1) at a flow rate of 60 mL/min. Eluting fractions, detected at 214 nm, are collected, and injected onto analytical column as described above. Fractions containing the pure target peptide were then combined and lyophilized. Qualification data for all synthesized peptides are listed on **Tables 1a** and **1b** together with their respective sequences. Non-standard Fmoc-amino-acid building blocks are listed in **Table 2.**

2.6 Peptide sample preparation: All peptides were classically solubilized in pure DMSO at 100 mM (net peptide content). Then, a 10x working concentration was reached by diluting the stock solution in PBS buffer. For each solution, we tested the number of particles in the solution to survey the possible aggregation by light scattering measurements at 400 nm as previously described [24]. No aggregation was detected under our experimental conditions in the 10x solutions.

2.7 FLIPR^{TETRA} instrument: The FLIPR Tetra system (Molecular Devices, Sunnyvale, CA) with whole-plate imaging allows the measurement to be accomplished in a 96-well format with well-by-well analyses, video archiving of data, and automated data analysis. The system has an on-board liquid handling for dispensing simultaneously into the 96 wells of the plate, compound(s) or reagent(s) from dedicated plates or vials. These additions are time controlled. Incidentally, the variation on pipetted volumes was measured to be less than 0.2%. The acquisition of the data in the instrument is made easy by the use of plates in which the entire bottom is illuminated with excitation light and then fluorescence emission is imaged onto a fast CCD camera. The signal from individual wells is discerned by appropriate binning of pixels associated with each well, and the average intensity is recorded as a function of time. This allows kinetic measurements to be performed on a well-by-well basis with superior signal to noise ratio. This allows dosing to be controlled very accurately from both a volume and timing perspective [12]. Each well is considered as a single timely measure.

2.8 PMCA-dependent Ca^{2+} traffic measurement: HEK 293 cells, cultivated as described [25], were seeded on poly-D-Lysine coated 96-well plates (Corning, Sigma Aldrich) 24 hours before the assay at a density of 40,000 cells/well in PBS buffer. Cells were then loaded for 1 hour with 5 µM Rhod-4-AM (Molecular Devices, San José, CA, USA) as previously described [26] in the presence of 20 µM sulfinpyrazone (Sigma-Aldrich), an anion transport blocker [27]. The design of the experimental protocol is described in the corresponding paragraph (see Results section). The cytosolic calcium-related fluorescence, subtracted from the baseline level, was measured at 555 nm (λex = 488 nm) for up to 15 minutes at room temperature. All measurements were performed with the FLIPR-TETRA instrument in quadruplicates (with some experimental variations) and independently repeated (n = 3-6). Up to the point where the experimental test parameters were validated, we present the data as direct measurements of the fluorescence due to the Rhod-4/Calcium complex.

Once the various parameters were fixed, the data were converted as follows (**Scheme 2**). Measuring the baseline during 10 sec in each well before the addition of the test compounds, the instrument established the baseline control from each well, and subtracted it to the assay measurement, for each individual well. It then transformed this data into an area under the curve (AUC) during the time of the experiment (ending after 15 minutes). This value was taken as representative of the effect of the test compound on the calcium efflux. Each value was thus the mean of the effect of the test compound on 40,000 cells measured at least in triplicate. The effect of PMCA inhibitors was evaluated by subtracting the AUC of the condition without inhibitor from that of with inhibitor (each of them being its own control measured before adding the compound). Delta AUC (ΔAUC) were plotted against concentrations of the inhibitor candidate, the higher the value of the ΔAUC was, the better the inhibitory activity. A PMCA unspecific inhibitor, ortho-vanadate – oVa –, was tested on each plate at concentrations ranging from 10^{-5} to 10^{-2} M as positive control (see Results section for full description).

2.9 Statistical analysis: ΔAUC data, expressed as mean ± SEM, were analyzed with Prism Software (Graphpad Software, San Diego, CA, USA) and considered significant as follows, $*P < 0.05$, $**P < 0.01$ or $***P < 0.001$.

3. Results

3.1 Design of a pharmacological assay to assess the PMCA function. The assay was based on cytosolic calcium fluorescence recording from HEK 293 cells that express mainly PMCA4 and only traces of PMCA1 [4,7].

In a living cell, the cytosolic calcium originates either from intracellular store release or extracellular importation. One can regard the cytosolic calcium concentration as the result of a balance between two opposite processes (**Scheme 1A**). The Ca^{2+} that permeates from the endoplasmic reticulum (ER) through IP_3 receptors (IP_3R) [28] and ryanodine receptors (RyR) [29] as well as from mitochondrial calcium fluxes [30] and Na/Ca-exchanger (NCX) [31] and from the transmembrane channels or transporters tends to increase calcium cytosolic concentration while PMCAs and calcium uptake into the ER *via* the sarco-endoplasmic reticulum Ca^{2+} ATPases (SERCAs) lead to its reduction. PMCA and SERCA are the major Ca^{2+} clearance pathways in most non-excitable with other Ca^{2+} fluxes such as mitochondrial Ca^{2+} fluxes, NCX and other Ca^{2+} channels/transporters contributing either no or a minimal role in maintaining steady state Ca^{2+} homeostasis [32].

Therefore, we aimed at reaching an experimental condition where the cytoplasmic calcium is high, the extracellular calcium influxes are blocked, and their uptake mechanism abolished. When measuring the concentration of the cytosolic calcium *via* a specific intracellular fluorescent probe in this situation, a descending fluorescent signal would reflect mainly the PMCA-dependent calcium extrusion activity which is the core of our study. The Rhod-4 probe was preferred to Fluo-8 indicator because of its higher dynamic response to calcium. This choice did not permit to use the ruthenium red to inhibit mitochondria calcium import so we cannot rule out its intervention in our assay. However, caloxins do not interact with intracellular processes due to their peptide nature that limits their action to the extracellular side. The effects studied in this assay should then rely only to transmembrane effector regulation, *i.e.* theoretically PMCAs.

Thanks to the benefit of several decades of calcium homeostasis studies, numerous chemicals have been characterized to block cellular calcium fluxes operated by channels and pumps. Experimentally, the initial step which was to empty the internal ER stores of HEK 293 cells was achieved by applying 10 µM of 2-benzyl-3-[hydroxy-(2-phenylacetyl)amino]propanoic acid (*a.k.a.* cyclopiazonic acid, CPA, a blocker of the ER calcium uptake SERCAs [33]) in a calcium-free medium. As a second step, the addition of extracellular calcium ($CaCl_2$) to a final concentration of 1.2 mM, then triggered a rise of the cytosolic calcium carried principally by the opening of ORAI, a transmembrane calcium channel opened by intracellular store depletion (Store-Operated Calcium Entry, SOCE [34]). At this point, due to the SERCA inhibition by CPA the ER remains depleted and the continuous activation of ORAI channels and other minor calcium influxes should be stopped to reveal the PMCA calcium extrusion activity. The efficacy of different calcium entry blockers was

studied by challenging the pharmacological sensibility of the rise in cytosolic calcium following external calcium addition after complete internal calcium depletion. For this purpose, the addition of extracellular calcium was accompanied with increasing concentrations of different standard Ca^{2+} entry inhibitors in the presence of CPA (**Figure 1A**). Among the various Ca^{2+} entry blockers tested (oVa, $NiCl_2$, $CdCl_2$, SKF96365, S66, econazole and 2-APB), Ni^{2+}, S66, econazole and 2-APB efficiently blocked almost entirely the increase in fluorescence induced by the 1.2 mM Ca^{2+} solution, indicating that calcium entry was nearly abolished. Despite 2-APB displaying some variations at µM doses (**Figure 1A**), we selected this inhibitor for safety, availability, and supply cost reasons. As variations might be due to a residual 2-APB-resistant Ca^{2+} entry, the assay was further optimized by testing the remaining calcium inhibitors in combination with 2-APB. As shown (**Figure 1B**), Ni^{2+} concentration-dependently prevented residual cytosolic calcium increase in the presence of 50 µM of 2-APB. The increase in fluorescent signal at high concentrations for SKF 93365 and Cd^{2+} can be attributed to solubility issues and to chelation with Rhod-4 indicator, respectively. In summary, after attempting the use of a series of experimental maneuvers to inhibit the calcium fluxes, the most accurate condition for assessing PMCA function was obtained by a combination of the Ca^{2+} entry blockers, 2-APB and $NiCl_2$, in the presence of CPA according to a final protocol summarized in **Scheme 2**.

In these conditions, this assay allows to measure mostly the strict PMCA-dependent decrease in the cytosolic calcium in a screening-friendly format under a FLIPR experimental setup. For the evaluation of PMCA inhibitor candidates, we used oVa as an internal and systematic reference compound. We chose oVa because *(i)* it was much more often used than the other ones, and *(ii)* carboxyeosin is a potent fluorophore [35] that would interact with Rhod-4 measurements, leading to misinterpretations. oVa was used at concentrations ranging from 10^{-5} to 10^{-2} M. Above 10^{-3} M, its specificity of action is however uncertain particularly regarding phosphorylation and dephosphorylation events. Indeed, vanadate is known for decades to inhibit kinases and phosphatases [36–38]. Prototypical traces of fluorescence recordings are presented in **Figure 2A**. Concentration-response curves are finally built by plotting AUC variation as a function of the concentrations of the test compounds as exemplified for oVa and **cal1b1** (**Figure 2B**).

3.2 Practical description and considerations. Cells were seeded and 24 h later, loaded with 5 µM Rhod-4 in the presence of 20 µM sulfipyrazone as described above. Rhod-4 was preferred over other calcium fluorescent indicators essentially because it is a good probe of cytosolic calcium, in various situations [26]. At the end of the loading procedure, cells were resuspended in a Ca^{2+}-free 10 µM CPA solution. After 10 min of baseline measurements, the cells were challenged with a caloxin derivative or oVa in the presence of 1.2 mM $CaCl_2$, 50 µM of 2-APB and 300 µM $NiCl_2$ in PBS buffer (**Scheme 1C**). Typical recorded profiles are presented in **Figure 3A** that represents a FLIPR screen-

copy of a single plate measurement, in real time. **Figure 3B** shows the first 3 minutes of the recording, during which turbidimetry leads to undershooting traces (below zero). These fluorescence traces appear to be dynamically changing over time, most likely due to variations in Ca^{2+} fluxes and minor turbidity changes due to addition of reagents. However, any difference in baseline control condition (without PMCA inhibitor) compared to following the addition of putative peptides can be assumed to be due to inhibition of PMCA leading to an increase in resting Ca^{2+} concentration. Therefore, any difference in AUC measured during these periods represents the degree of PMCA inhibition that can then be plotted as concentration response curves in all subsequent data.

The first layer of transformation was then the subtraction of the AUC of the baseline condition (before the addition of the compound) to the AUC recorded in the presence of the compound. This leads to a representation as shown in **Figure 3C** (right panel). This figure depicted the automatically obtained graph of the kinetical action of any individual compound, as calculated thanks to a FLIPR dedicated function [39]. This data was transformed a second time as follows: The AUC, as it remains after the subtraction of the baseline (to each point), was considered as the value of reference for the effect of the compound. This data was then constructed as a plot as a function of the various concentrations tested, most of the time from 1 to 100 µM, in the routine format. A representative plot is shown in **Figure 3C** for some compounds studied as actual examples of the whole process. Note that for every compound at least 3 curves were recorded per tested concentration and transformed to lead to a final number with its standard variation.

At that stage, the assay was consolidated and was ran as described in **Scheme 1C**. The compounds were tested in the presence of CPA (10 µM), 2-APB (50 µM) and Ni^{2+} (300 µM) in PBS buffer. From now on, the system is setup in a way that permit to calculate directly the ΔAUC. Although we cannot completely rule out a minor component from additional Ca^{2+} fluxes contributing to the measured AUC, we can assume that these may be the same during the baseline *versus* treatment periods. Therefore, the ΔAUC is the best estimate of PMCA inhibition that combines the convenience and power of a high throughput screening of large numbers of putative PMCA inhibitors

3.3 The evaluation of a first series of caloxin1a, -1b, -1c, -2a and -3a derived peptides. Our first set of experiments was to validate the data published for the reference caloxins -1a, -1b, -1c, -2a and -3a (**Table 3**) in our own system. The **cal1b1**, **cal1b3**, and **cal1c2** variants were originally described with the best activities [20]. In our cellular system, we found **cal1b1** and **cal1b3** to perform modestly at 30 µM, but better than all the other caloxins tested herein (**Figure 4** and data not shown), somehow validating the accuracy of our PMCA-based assay. These peptides were less efficient but

600 to 1000 times more potent than oVa (EC_{50} from 17 to 30 µM versus 30 mM). To the best of our knowledge, these peptides, once discovered by phage display, were not optimized and analogues were not reported in the literature review [20]. Our choice was to start by exploring the most obvious steps in peptide medicinal chemistry for both **cal1b1** (TAWSEVLHLLSRGGG-NH_2) and **cal1b3** (TIPKWISIIQALRGGGSK-NH_2). Indeed, we disregarded **cal1c2** because this caloxin was as active as **cal1b3** in our hands (data not shown) and this peptide is an analogue sequence-wise of the two previous ones. Thus, we reasoned that the structural message borne by the **cal1c2** should be kept in **cal1b1** and **cal1b3**. For the sake of simplicity, we adopted a nomenclature inspired from the previous research published on caloxins: the parent compound name, *e.g.,* **cal1b1**, is followed by its analogue number, following the order of synthesis such as **cal1b12**, **cal1b13**, or **cal1b31**, **cal1b32** and so on. To start implementing a peptide-driven classical approach to analogues of **cal1b1**, we synthesized a series of analogues aiming at finding the shortest active sequence.

To investigate the contribution of the N-terminal residue, the Trp moiety and the C-terminal region of **cal1b1** in PMCA-mediated Ca^{2+}-efflux inhibiting activity, we have generated point-substituted and down-sized analogues of the peptide (**Table 4**, **cal1b1**-**cal1b16**). Deletion of the three contiguous C-terminal Gly units (**cal1b11**) or their substitution by a 6-aminohexanoic acid (**X6**) moiety (**cal1b12)** did not affect the biological activity of the peptide (**Figure 5A**). Similarly, replacement of the Trp residue in position 3 of **cal1b1** by classical counterparts such as 2-naphthyl-alanine (**X7**) or β-(benzothiazolyl)-alanine (**X16**) led to **cal1b13** and **cal1b14** as potent as the lead peptide. Finally, N-terminal acetylation of the Thr residue or its substitution by azetidine-2-carboxylic acid (**X9**) did not improve the PMCA inhibiting property of **cal1b1** (**cal1b15** and **cal1b16**). Since no significant improvement was obtained in PMCA inhibition with **cal1b1** analogues, we turned to **cal1b3** for a similar approach aiming to find the smallest active sequence (**Table 5**).

Figure 6 shows that successive deletions of 1 to 5 C-terminal residue(s) did not affect the biological activity of the peptides (**cal1b31** to **cal1b35**). However, additional deletions of Arg^{13} (**cal1b311**), Leu^{12}-Arg^{13} (**cal1b312**) and Ala^{11}-Leu^{12}-Arg^{13} (**cal1b313**) markedly reduced the potency of **cal1b3** analogues. Similarly, N-terminal truncations of 1 to 5 amino acids of either **cal1b3** (**cal1b36** to **cal1b39** and **cal1b310**) or **cal1b35** (**cal1b314** to **cal1b316**) sequences yielded less potent analogues (**Figure 6**). This loss of activity is particularly marked for peptides shortened by at least 4 residues (**cal1b39** and **cal1b310**). Taken as a whole, **cal1b35** represents the iso-active sequence of **cal1b3** and was considered as a template for further optimization.

The contribution of Lys^4, Trp^5, Ser^7 and Gln^{10} side chains to the biological activity of **cal1b35** and close analogues was evaluated by systematic alanine replacements (Ala-scan) (**Table 6**). **Figure 7** compares the efficacy of all these compounds (30 µM) as PMCA inhibitors to oVa (10 mM). Globally,

all these peptide derivatives were less efficient than oVa. Among this series, the concomitant Ala-substitution of Ser^7 and Gln^{10} of **cal1b35** (**cal1b322**), its analog modified in position 1 by a γ-aminobutyric acid (**X1**; **cal1b327**) and its 3 N-terminal residue deleted counterpart (**cal1b340**) were the most active members, scoring in the 15 to 25% range inhibition compared to 100% of inhibition for oVa at a 3 orders of magnitude higher concentration. Interestingly, it appears that the beneficial effect of the double Ala-substitution in compounds **cal1b322** and **cal1b327** exceeded the loss of activity initially detected by the shortening of 3 residues in caloxin **cal1b316** in comparison to **cal1b35** since **cal1b340** was as potent as **cal1b322** and **cal1b327**. In order to design the shortest caloxin possible, we have continued our sequence optimization process on the structure of **cal1b340** (KWIAIIAALR-NH_2) with the proposed nomenclature of **cal1d** derivatives (**Table 1b**). As a first step, it was attempted to modify the N-terminus of this peptide, by entering in place of the Lys^1 residue two non-proteinogenic amino acids, either 2,4-diamino-butyric acid (**X13**) or 2,3-diamino-propionic acid (**X2**). Incorporation of these two building blocks resulted in a slight decrease in the activity of the corresponding peptides **cal1d19** and **cal1d20** at 30 µM (**Table 7**) in comparison to the starting **cal1b340** peptide. The substitution of the C-terminal arginine of **cal1b340** by an Ala moiety led to an almost inactive peptide (**cal1d21**), strongly enforcing the key nature of the basic charge at the C-terminus as previously suggested. Similarly, the substitution of the same residue by a lysine led to a diminished inhibitory capacity of the corresponding peptide (**cal1d22**) compared to the starting one (**cal1b340**). Finally, we synthesized an all-D version of **cal1b340**. The resulting peptide **cal1d23** was poorly active, barely 20% of the starting peptide activity at 30 µM.

3.4 Evaluation of caloxin1d derived peptides - Central region. We have shown above that the central residues of **cal1b340** (-IAIIAA-) tolerated particularly well their substitution by an alanine with minor loss of activity suggesting this region acted as a spacer between both extremities where alanine replacement led to a loss of PMCA inhibition. Thus, **cal1b340** can be regarded as a 3-zone delineated sequence: a N-terminal KW motif, a long stretch of alkyl-side-chain-bearing amino acids (isoleucine and alanine) and a C-terminal dipeptide leucine-arginine, the later with a positively charged guanidino group (**Figure 8**).

We first explored the central zone corresponding to the aliphatic, rather hydrophobic and extended region -IAIIAAL-, by substituting this sequence by different spacers of various length. Description of the linkers inserted within the **cal1b340** sequence leading to **caloxin1d** analogues and their respective PMCA inhibiting activity are reported in **Table 8**. Noticeably, the dipeptides KW-NH_2 (**cal1d69**) and LR-NH_2 (**cal1d68**) as well as an equimolar mixture of the dipeptides (**cal1d70**) did not exhibit any

inhibiting activity in our model of PMCA functionality demonstrating the pivotal role of the linker between these two parts. With the aim to understand the optimal structure/length of this extended region in **cal1d**, we selected a series of building blocks to vary the length between the N- and C-terminal extremities from 3 to 24 heavy atoms in the backbone. Most of the attempts failed, leading to **cal1d** derivatives with weak - if any - inhibitory property towards PMCA-mediated calcium movements (**Table 8**). Surprisingly, **cal1d16** and **cal1d17** which encompassed spacers as long as the parent peptide **cal1b340** with a comparable hydrophobicity pattern were totally devoid of activity as well as caloxins with shorter but similar linkers (**cal1d14**, **cal1d15** and **cal1b342**). This feature was also seen in a few previous data, in which Ala-substitution led to many peptides with null activity such as **cal1b39** and **cal1b334**, among many others (**Figure 7**). This feature was somehow contradicted by the finding of the possible replacement of this central core by a single amino acid, in which the succession of N-Cα-CO moiety was absent. Indeed, the optimum size of the linker was in the 13-atom range, as seen for **cal1d1,** encompassing a 12-amino-dodecanoic acid moiety (**X5**), which was as potent as **cal1b340** at 30 µM. Longer or shorter versions failed to enhance the inhibitory capacity of the corresponding peptides, as exemplified by compounds **cal1d47** and **cal1d13** containing 15-amino-pentadecanoic acid (**X20**) and 5-amino-pentanoic acid (**X11**) residues, respectively. We have also introduced the **X5**LR motif on the side-chain amino ε group of the KW-NH_2 dipeptide. Surprisingly, the resulting branched peptide **cal1d54** K(**X5**LR)W-NH_2 retained about 50% of the activity of the linear parent peptide (Δ AUC 435 ± 78 *vs.* 573 ± 94 for **cal1d1**).

In this series, we also verified that the leucine moiety was mandatory and could not be directly included in a longer amino-acid linker such as 15-amino-pentadecanoic acid (**X20**) present in **cal1d48**, which encompasses the 12 heavy atoms of 11-amino-undodecanoic acid (**X4**) and 4 extra ones corresponding to almost the 3 heavy atoms of the leucine backbone of **cal1d11**. The same approach was applied by substituting the -IAIIAA- hydrophobic scaffold by 15-amino-4,7,10,13-tetraoxa-pentadecanoic acid (**X19**, amino-$(PEG)_4$-carboxylic acid) moiety in **cal1d39** for comparison with a "PEG_3"-containing **cal1d37** (**X15**, 12-amino-4,7,10-trioxa-dodecanoic acid). In both cases, this modification had little effect on the potency of the corresponding peptides.

The full retro sequence of **cal1d1** was also prepared in which the peptide backbone corresponded to the anti-wise sequence RL**X5**WK-NH_2 (**cal1d79**). Not surprisingly, **cal1d79** was at least as active as the parent compound (data not shown), strongly suggesting that the scheme of **Figure 8** is confirmed and that the central zone only plays an "addressing" role for both terminal parts. Finally, the retro-inverso analogue, **cal1d80** (rl**X5**wk-NH_2), displayed a higher inhibiting activity than **cal1d1**. Surprisingly, this result is at the odd of that of obtained with the all-D peptide **cal1d23**, the retro-inverso version of **cal1b340**, that lost more than 90% of the activity (**Table 7**).

At this stage, **Figure 9** shows the inhibiting activities of the 2 most interesting caloxins **cal1b3** and **cal1d1** in comparison to the reference inhibitor oVa. The short caloxin **cal1d1** was at least as active as **cal1b3** and exhibited an efficacy at 100 µM that could be useful for a reference PMCA inhibitor. Therefore, we kept the structure of **cal1d1** as a model for further explorations.

In further attempts to better understand the structure-activity relationship of these **cal1d1** derivatives, we synthesized other centrally modified caloxins containing cycle or branched alkyl backbones between the KW- and -LR-Nus. These peptides necessitated the synthesis of the Fmoc-protected non-natural amino acids (**Table 2**) and those results came very late in the program, somehow impairing the design of new analogues. With the exception of compound **cal1d67**, these caloxins were better inhibitors at 30 µM than the parent peptide **cal1d1** (**Table 9**). However, considering the difficulties of access to those amino acids), the **X5** linker was chosen for the following steps of optimization.

3.5 Evaluation of caloxin1d1 derived peptides – N-terminal extremity. We continued the optimization of the **cal1d1** sequence by detailing the properties of its N-terminal extremity (region 1), *i.e.,* the lysine-tryptophan dipeptide. **Table 10** summarizes the various substitutions and the results obtained with the corresponding peptides on the PMCA-mediated calcium movement in our model at 30 µM. As demonstrated above, we maintained the distance between zones 1 and 3 at 12 heavy atoms by systematically (with the exception of **cal1d41**) using 12-amino-dodecanoic acid (**X5**) as a spacer. Acetylation of the N-terminal extremity of compound **cal1d1** had a strong detrimental effect onto the inhibitory potency of **cal1d51**. An unexpected solubility issue cannot be totally ruled out at the stage, **cal1d51** being significantly more hydrophobic than **cal1d1**. Similarly, replacement of the Trp moiety by a His residue led to peptide **cal1d27** totally devoid of inhibitory capacity, whereas changing into Tyr (**cal1d45**) or Phe (**cal1d44**) had fewer radical effects. Substitution of the Lys residue by Orn or Dab units did not drastically affect the potency of the corresponding analogues **cal1d30** and **cal1d29**, respectively, even though a slight enhancement could be noted for one methylene shortening in the side chain of lysine. Intriguingly, further side-chain methylene shortening yielded the Dap-containing **cal1d28** which presented the best inhibiting activity of this series. When the nature of the amino acid was changed (basic for Lys for neutral Gly or Ala, like in **cal1d76** or **cal1d77**), the respective resulting activities were not drastically changed from **cal1d1**, but when the length of the side chain is maintained (Lys and n-Leu), the activity remains in the 700 Δ AUC range. Finally, replacement of the Nε amine side chain function of lysine by a carboxylic acid function (**X36**) in **cal1d83**, or by a -CH_2-COOH group (**X27**) in **cal1d84** greatly reduced the activity of **cal1d1** in the same way as the loss of N-terminal amine function (**X6**) in **cal1d85**.

3.6 Evaluation of caloxin1d derived peptides – C-terminal extremity. Because of the non-polar, aliphatic, and bulky nature of the leucine sidechain, the possibilities of incorporating

455 counterparts into the C-terminal LR dipeptide were limited (**Table 11**). The leucine in **cal1d1** can be
456 changed without major differences in the PMCA inhibiting activity by hydrophobic amino acids such
457 as Ile (**cal1d87**), its straight-chain analogue norleucine (**cal1d88**) or, more surprisingly, the shorter and
458 functionalized homo-Cys (**cal1d89**). Finally, substitution of the C-terminal arginine by its
459 homologated version, homo-Arg, led to a significant reduction in the activity (**cal1d31**), whereas
460 dimethylation of the guanidino group (**X25**), its protection by a nitro function (**X26**) or its substitution
461 by an ureido group (**X24**) almost nullified the inhibiting activity of **cal1d58**, **cal1d59** and **cal1d56**,
462 respectively. None of these three compounds were more potent than their parent **cal1d1.** Noticeably,
463 **cal1d56,** was practically inactive pointing out to a key role of the guanidino moiety of arginine as
464 opposed to the ureido group of citrulline (**Table 11**).

4. Discussion

The use of improperly characterized pharmacological tools is a source of confusion and misleading results. The literature is full of use of inhibitors in cellular conditions that have never been characterized for their actions in such a context. Another type of examples is the use of antagonists at G-protein coupled receptors in vivo, while their stability and their uptake have never been studied (see our discussions for example in Boutin & Legros [40] or in Boutin et al. [41]). This is one of the main reasons why we attempted the present research campaign using a living system. Another aspect is the challenging access to purified integral membrane proteins, such as GPCRs [42] and channels .

The extraordinary diversity of tools, more or less characterized in terms of stability and/or specificity, led us to the possibility to create a pharmacological model in which only our target protein, PMCA - presumably PMCA4 -, was functionally active. Indeed, our interpretation of this system is as follows: CPA blocks SERCAs leading to a net efflux of an irreversible leak of Ca^{2+} from the RE to the cytosol. The cellular compensatory response leads to the opening of ORAI to promote extracellular calcium entry to refill the RE, system nevertheless blocked due to the inhibition of SERCAs by CPA. Therefore, under those conditions, the only actors left for the Ca^{2+} homeostasis are ORAI and PMCA. Finally, the function of ORAI is blocked by the addition of 50 µM 2-APB. The net result of this pharmacological manipulation of the different actors of the Ca^{2+} led to the measurement of cytosolic Ca^{2+} accumulation depending only on the capacity of PMCA to exclude Ca^{2+} from the overconcentrated cytosol (**Scheme 1**).

Small molecules, in particular synthetic compounds, are often coming from the analogizing of natural products [43]. For example, more than a thousand analogues of melatonin as melatonin receptor agonists, were designed in a somewhat rational approach [41]. Alternatively, one can perform HTS campaigns permitting to discover *de novo* structure(s) with potent antagonist or inhibitory capacities with chemical structures unrelated to the natural ligand or substrate/co-substrate of the targeted protein. This situation is slightly different whenever compounds issued from natural sources (particular from plant extracts) are screened and new candidates discovered from this origin. As discussed in Lautié et al. [43], a common feature of natural products is that they statistically recognize a smaller number of protein targets per molecule than synthetic ones (in a roughly 3 to 6 ratio).

Finally, peptides form a third category of chemicals that often offer two advantages that are probably inter-dependent: (*i*) they are built of simple bricks that are similar and/or identical to those making the proteins, offering theoretically a better "guarantee" of specificity because they are slightly larger than the common synthetic compounds (see discussion in Gruber et al [44]). Therefore, one can hypothesize that by enhancing the number of contacts between the chemical and the targets, one can hope a more intimate complementarity and, therefore, less off-target affinity for unrelated proteins. (*ii*)

Peptides offer an almost infinite number of analogues because it exists literally hundreds of amino acids that can be integrated in the starting sequence with the relative simplicity of solid phase synthesis. Several in depth views of the specificity of peptides has been done and computerized (see for example Bhattacherjee and Wallin [45]). They would argue that the complexity of the binding of peptides onto a protein target is dependent on too numerous parameters that only *in silico* simulations [46] and/or co-crystallization of their complex [47] can reveal.

The next level of difficulty is then the starting points. Roughly three sources of peptides can be discovered: the combinatorial library approach [48,49], the analogues to the natural ligand [50] and the phage display approach [51]. To these sources, could be added the use of peptides included in massive screening campaigns as part of the global chemical sources of hits in the HTS approach, although quite often, the discovery of peptides as hits in such campaigns is disregarded to the profit of smaller organic chemicals at least in the pharma industry that is the main source of such campaigns.

PMCA is a key component of the calcium homeostasis of the cells. PMCAs have been linked to many pathological situations [see [5] for complete review]. The main pharmacological tool used in this area remains *ortho*-vanadate. This compound has been described for ages as a strong inhibitor of PMCA [52]. It is considered an analog of phosphate and has been reported numerous times for its capacity to inhibit kinases and phosphatases rendering its use difficult in a living system, including in cells.

Several compounds were reported following HTS campaigns on this PMCA target [21]. For example, aurintricarboxylic acid was discovered during such a campaign [53]. This polymeric dye is typical of HTS campaign findings. Indeed, this compound was also reported over the years as an inhibitor of protein-nucleic acid interactions, a potent inhibitor of ribonuclease and of topoisomerase II [54]. It also stimulates tyrosine phosphorylation processes, probably by inhibiting phosphatase(s) [55]. Finally, it inhibits apoptosis [56,57], prevents the downregulation of GluR2 receptors [58] and inhibits calpain, a Ca^{2+}-activated protease that is activated during apoptosis [59]. It is important to point out that this compound could not be defined as a specific inhibitor at PMCA [60]. In the 1980s, Grover group applied the technique of phage display to screen for alternate inhibitors with peptide structures and found a series of peptides from 12 to 20 amino acid long (see **Table 1a**) [16]. No report on the optimization of those peptides was reported in the literature.

As stated above. small organic chemical could be interestingly challenged by peptides or pseudopeptides [61] or natural compounds [43] because those compounds are potentially more specific of a given target than the former ones. We thus embarked in a long program aiming at finding smaller alternative compounds to the caloxins already described by Grover's group [16]. The main purpose of the study was indeed to find a more practical (*i.e.,* shorter) peptide that could be used in studies on PMCA-dependent Ca^{2+} movement in cellular contexts. One should recall that the longer the

peptide (or the heavier the organic compound), the more costly and complicated its synthesis will be. Introducing such a size parameter in pharmacological research is also the first step towards rationalizing the future and possible passage from an experimental compound usable in research to a druggable compound aiming at therapeutical purpose. Furthermore, in more fundamental considerations, peptide structures are uneasy to obtain in crystallization experiments, and the common lack of structural information on active peptide is also a limit to their use [61]. Finally, a discussion still exists on whether a shorter compound would be more as opposed to less specific of its target, because it retains less structural information than their longer counterpart(s).

We applied a simple step by step classical strategy by which we (*i*) defined the best starting point under our experimental conditions; (*ii*) applied the standard shortening of the peptides; (*iii*) tried to define the final molecule using simple concepts. Final peptides were already a great step from the initial caloxin (*i.e.,* **cal1b3**).

Finally, two other parameters were measured but not considered: the height of the Ca^{2+} peak and the duration of that peak. These parameters would permit to finely evaluate, and these data are gathered in a supplementary table for the main peptides issued from the present sets of experiments.

As a conclusive remark, one should first point out to the relative value of data obtained in living cells – or in living animals – where repetitions from experiments to experiments remain often within a large variation interval. To limit this fact, we chose two ways: *(i)* we only compare results obtained within a set of experiments run the same days, at multiple occasions, often at least three different plates containing each triplicate of a same experiment. These are the numbers one can find in tables. In these cases, the present variation was generally below 10%; and *(ii)* we express at the end of the experiment the main results in a format considering for the 15 "best" peptides the ratio to both **cal1b3** and **cal1d1** results obtained in the same experiments as well as, for these same peptides, an IC50 approximated from 3 concentration values of the set of experiments (**Table 12**). This list is a summary and an indication of the next steps that should be undertaken to further qualify the "best" peptides. For example, the assessment of the stability of the candidate could be predicted – the all-D peptide: **cal1d80** should be a strong candidate – but the actual data is missing. On the other hand, we did not have the opportunity to screen all the candidates in a single set of experiments, where their potencies could be expressed relatively to each other and to the initial **cal1b3**. Finally, one can wonder if the best candidate(s) would be specific enough of a set of relevant off target proteins and channels.

Of course, despite a cellular approach – that is, a living system, – these molecules are far from a perfect tool to study PMCA-mediated Ca^{2+} movements in a more complex system and even farer from a candidate to solve therapeutical problems. Nevertheless, there are good and simpler candidates on which further hit-to-lead strategies will be applicable.

5. Conflicts of interest

The authors declare no competing financial interest.

6. Acknowledgments

JAB would like to thank the team from FluoFarma (M. Petit, L. Cerf, F. Ichas and F. di Giorgi) for the help with this work. The authors are indebted to an anonymous referee whom helped them greatly presenting the work.

7. Author contribution:

JAB. Conceptualization, Peptide design, Pharmacological experiments, Data curation Writing, original, review & editing; LF: Peptide design; SB: Pharmacological experiments, Data curation, Writing, review & editing; MJ: Peptide design, Writing, review & editing; MG: Writing, review & editing, PG: Peptide design; GF: Pharmacological experiments, Data curation Writing, review & editing; KP: Peptide design, Writing, review & editing; JL: Data curation, Writing, original, review & editing.

8. Legends to the figures

Scheme 1: Calcium homeostasis in a mammalian resting cell and pharmacological window for PMCA function assessment.

A. Simplified schematic representation of Ca^{2+} dynamics in a mammalian resting cell;
Cytosolic Ca^{2+} concentrations are maintained at nM levels against a more than 4 orders of magnitude higher levels in intracellular stores and extracellular space. Orchestrated actions regulate calcium homeostasis summarized by proteins able to (i) either pump calcium ions out from cytosol to the extracellular milieu (PMCA) or into intracellular stores such as ER (SERCA) and (ii) fill out the cytoplasm by reverse action involving ORAI and IP_3R/RyR, respectively.

B. Schematic representation of the pharmacological treatment for PMCA function assessment. In extracellular Ca^{2+}-free condition, CPA triggers ER store depletion; this calcium release in the cytoplasm induces STIM to couple with the plasma membrane Ca^{2+} channels ORAI for refill (store-operated calcium entry process). Extracellular calcium demand is supplemented by addition of $CaCl_2$. Concurrently, treatment with 2-APB blocks ORAI calcium entry. Mitochondrial calcium leak is prevented by addition of Ni^{2+} (not shown).

Figure 1: Validation of reference compounds

Design of the pharmacological window for PMCA function assessment in HEK 293 cells. **A**, Effect of calcium entry inhibitors on intracellular calcium concentration of HEK 293 cells obtained in the presence of CPA (10 µM). Representative concentration-response curves for $NiCl_2$ (orange closed circle), $CdCl_2$ (red closed square), SKF 96365 (blue closed triangle up), S66 (green closed triangle down), econazole (purple closed diamond) and 2-APB (black open circle). Blue closed star represents the signal in calcium-free condition. Data are mean ± SEM of triplicate from, at least, three independent experiments. **B**, Effect of calcium entry inhibitors on intracellular calcium concentration of HEK 293 cells obtained in the presence of CPA (10 µM) and 2-APB (50 µM). Representative concentration-response curves for $NiCl_2$ (orange closed circle), $CdCl_2$ (red closed square), SKF 96365 (blue closed triangle up), S66 (green closed triangle down) and econazole (purple closed diamond). Blue closed star represents the signal in calcium-free condition. Data are mean ± SEM of triplicate from, at least, three independent experiments.

Figure 2: Calcium kinetics in HEK 293 cells.

A, Changes in cytosolic calcium content (normalized fluorescent intensity units) of HEK 293 cells measured in FLIPR assay over a period of 30 min (15,000 sec). Examples of kinetic profiles of different caloxin analogues obtained in the presence of CPA (10 µM), 2-APB (50 µM) and Ni^{2+} (300 µM). The AUC during the control condition (without PMCA inhibitor) can be subtracted from the AUC with the putative PMCA inhibitor to give ΔAUC. This ΔAUC represents the degree of PMCA inhibition and is thus the basis of all subsequent concentration-response curves. Grey curve, solvent (control).

B, Effect of PMCA inhibitors on intracellular calcium concentration of HEK 293 cells. Representative concentration-response curves for oVa (black open circle) and **cal1b1** (red closed square) obtained in the presence of CPA (10 µM), 2-APB (50 µM) and Ni^{2+} (300 µM). Data are mean ± SEM of triplicate from, at least, three independent experiments.

Figure 3: Practical representations of the various steps of PMCA-dependent calcium efflux measurements.

A, Representative FLIPR traces of the PMCA-based measurement in HEK 293 cells. Half-log diluted concentration-response traces are displayed from row A (10 µM) to row G (0.01 µM). 0 concentration replicates are H01, H02 and H03. Columns 1-3 **caloxin 1b3**, columns 4-6 **caloxin 1b34**, columns 7-9 **caloxin 1b35**, columns 10-12: **ortho-vanadate** (oVa).

B, Comparison of kinetic measurements of the inhibition of the PMCA-driven efflux of Ca^{2+} in HEK 293 cells by various comopounds at a single concentration. Typical FLIPR traces recorded during the first four minutes

C, Examplification of data transformation from kinetic traces to ΔAUC graph. Left panel: comparison of kinetic measurement of the inhibition of the PMCA-driven efflux of Ca^{2+} in HEK 293 cells by 4 differents compounds at 30 µM. The grey trace displays solvent effect (control). Comparison of concentration-response curves for the same 4 different compounds (same color codes). Right pannel: the areas under the curve (AUC) were calculated and plotted *versus* the concentration of the compound.

Scheme 2: Schematic representation of the experimental setup.

HEK 293 cells are seeded in 96-well plates as indicted in the Material and Methods section (C1). After 18-24 h, cells are loaded with 5 µM of the calcium probe Rhod-4-AM in the presence of 20 µM sulfinpyrazone (C2). One hour later, fluorescence recording started (C3) just before triggering the ER

depletion with 10 µM CPA treatment (C4) for 10 minutes in Ca^{2+}-free condition. Then, cells are challenged by 50 µM 2-APB, 300 µM $NiCl_2$ and 1 mM $CaCl_2$ in PBS buffer concomitantly with graded concentrations of caloxins or oVa as positive control (C5) for at least 15 minutes of fluorescence measurement (C6).

Figure 4: Effect of reference caloxins on PMCA intracellular calcium concentration of HEK 293 cells compared to the classical PMCA inhibitor, ortho-Vanadate.

A, Representative concentration-response curves for oVa (black open circle), **cal1b1** (blue closed triangle up) and **cal1b3** (red closed square) obtained in the presence of CPA (10 µM), 2-APB (50 µM) and Ni^{2+} (300 µM).

B, Representative concentration-response curves for oVa (black open circle), **cal2a1** (red closed square), **cal3a1** (blue closed triangle up) and **cal3a2** (green closed triangle down) obtained in the presence of CPA (10 µM), 2-APB (50 µM) and Ni^{2+} (300 µM).

C, Representative concentration-response curves for oVa (black open circle), **cal1a1** (red closed square) and **cal1a2** (blue closed triangle up) obtained in the presence of CPA (10 µM), 2-APB (50 µM) and Ni^{2+} (300 µM).

Data are mean ± SEM of triplicate from, at least, three independent experiments. *p<0.05, **p<0.01 and ***p<0.001 vs. control condition as assessed by ANOVA and Bonferroni post hoc test. Reference caloxins were described by Grover [20].

Figure 5: Effect of caloxin 1b1-derived peptides on PMCA intracellular calcium concentration of HEK 293 cells compared to the reference caloxin 1b1.

A, Representative concentration-response curves for **cal1b1** (black open circle), **cal1b11** (red closed square), **cal1b12** (blue closed triangle up) and **cal1b13** (green closed triangle down) obtained in the presence of CPA (10 µM), 2-APB (50 µM) and Ni^{2+} (300 µM).

B, Representative concentration-response curves for **cal1b1** (black open circle), **cal1b14** (red closed square), **cal1b15** (blue closed triangle up) and **cal1b16** (green closed triangle down) obtained in the presence of CPA (10 µM), 2-APB (50 µM) and Ni^{2+} (300 µM).

Data are mean ± SEM of triplicate from, at least, three independent experiments.

Figure 6: Effect of caloxin 1b3-derived peptides on PMCA intracellular calcium concentration of HEK 293 cells compared to the reference caloxin 1b3 and classical PMCA inhibitor, ortho-Vanadate.

A, Representative concentration-response curves for **cal1b3** (black open circle), **cal1b31** (red closed square), **cal1b32** (blue closed triangle up) and **cal1b33** (green closed triangle down) obtained in the presence of CPA (10 µM), 2-APB (50 µM) and Ni^{2+} (300 µM).

B, Representative concentration-response curves for **cal1b3** (black open circle), **cal1b34** (red closed square), **cal1b35** (blue closed triangle up) and **cal1b36** (green closed triangle down) obtained in the presence of CPA (10 µM), 2-APB (50 µM) and Ni^{2+} (300 µM).

C, Representative concentration-response curves for **cal1b3** (black open circle), **cal1b37** (red closed square), **cal1b38** (blue closed triangle up) and **cal1b39** (green closed triangle down) obtained in the presence of CPA (10 µM), 2-APB (50 µM) and Ni^{2+} (300 µM).

D, Representative concentration-response curves for **cal1b3** (black open circle) and **cal1b310** (red closed square) obtained in the presence of CPA (10 µM), 2-APB (50 µM) and Ni^{2+} (300 µM).

Data are mean ± SEM of triplicate from, at least, three independent experiments. $^{**}p<0.01$ and $^{***}p<0.001$ vs. control condition as assessed by ANOVA and Bonferroni post hoc test.

Figure 7: Percentage of PMCA inhibition induced by oVa, reference caloxins cal1a1, -1b1, -1c2, -2a1, -3a1 and cal1b3 derivatives.

All caloxins except oVa were tested at 30 µM. (*) oVa was tested at 10 mM. Data are mean ± SEM of triplicate from, at least, three independent experiments.

Figure 8: Chemical structures of cal1b340, H-Lys-Trp-Ile-Ala-Ile-Ile-Ala-Ala-Leu-Arg-NH_2.

Caloxin **cal1b340** is organized in 3 successive parts, corresponding to a N-terminal KW motif, a central hydrophobic stretch and a C-terminal LR-NH_2 extremity.

Figure 9: Effect of new caloxin derived peptides on PMCA intracellular calcium concentration of HEK 293 cells compared to the reference caloxin 1b3 and classical PMCA inhibitor, ortho-Vanadate.

A, Representative concentration-response curve for oVa (black open circle), and 4 concentration-response curves for **cal1b3** obtained in the presence of CPA (10 µM), 2-APB (50 µM) and Ni^{2+} (300 µM).

B, Representative concentration-response curve for oVa (black open circle), and 4 concentration-response curves for **cal1d1** obtained in the presence of CPA (10 µM), 2-APB (50 µM) and Ni^{2+} (300 µM).

C, Two concentration-response curves for **cal1d53** obtained in the presence of CPA (10 µM), 2-APB (50 µM) and Ni^{2+} (300 µM).

D, Two concentration-response curves for **cal1d43** obtained in the presence of CPA (10 µM), 2-APB (50 µM) and Ni^{2+} (300 µM).

E, Two concentration-response curves for **cal1d28** obtained in the presence of CPA (10 µM), 2-APB (50 µM) and Ni^{2+} (300 µM). Data are mean ± SEM of triplicate.

9. References

[1] Strehler EE, Zacharias DA. Role of alternative splicing in generating isoform diversity among plasma membrane calcium pumps. Physiol Rev 2001;81(1):21–50. https://doi.org/10.1152/physrev.2001.81.1.21.

[2] Muallem S, Pandol SJ, Beeker TG. Calcium mobilizing hormones activate the plasma membrane Ca2+ pump of pancreatic acinar cells. J Membr Biol 1988;106(1):57–69. https://doi.org/10.1007/BF01871767.

[3] Brini M, Calì T, Ottolini D, Carafoli E. The plasma membrane calcium pump in health and disease. FEBS J 2013;280(21):5385–97. https://doi.org/10.1111/febs.12193.

[4] Bruce JIE. Metabolic regulation of the PMCA: Role in cell death and survival. Cell Calcium 2018;69:28–36. https://doi.org/10.1016/j.ceca.2017.06.001.

[5] Bruce JIE, James AD. Targeting the Calcium Signalling Machinery in Cancer. Cancers (Basel) 2020;12(9). https://doi.org/10.3390/cancers12092351.

[6] Niggli V, Carafoli E. The Plasma Membrane Ca(2+) ATPase: Purification by Calmodulin Affinity Chromatography, and Reconstitution of the Purified Protein. Methods Mol Biol 2016;1377:57–70. https://doi.org/10.1007/978-1-4939-3179-8_7.

[7] Glendenning P, Ratajczak T, Dick IM, Prince RL. Calcitriol upregulates expression and activity of the 1b isoform of the plasma membrane calcium pump in immortalized distal kidney tubular cells. Arch Biochem Biophys 2000;380(1):126–32. https://doi.org/10.1006/abbi.2000.1908.

[8] Preiss R, Banaschak H. Na,K-ATPase in excitation-contraction coupling of vascular smooth muscle from cattle. Acta Biol Med Ger 1979;38(1):83–96.

[9] Kreitzer MA, Collis LP, Molina AJA, Smith PJS, Malchow RP. Modulation of extracellular proton fluxes from retinal horizontal cells of the catfish by depolarization and glutamate. J Gen Physiol 2007;130(2):169–82. https://doi.org/10.1085/jgp.200709737.

[10] Chen Y, Cao J, Zhong J, Chen X, Cheng M, Yang J et al. Plasma membrane Ca2+-ATPase regulates Ca2+ signaling and the proliferation of airway smooth muscle cells. Eur J Pharmacol 2014;740:733–41. https://doi.org/10.1016/j.ejphar.2014.05.055.

[11] Pande J, Szewczyk MM, Grover AK. Allosteric inhibitors of plasma membrane Ca pumps: Invention and applications of caloxins. World J Biol Chem 2011;2(3):39–47. https://doi.org/10.4331/wjbc.v2.i3.39.

[12] Sirenko O, Crittenden C, Callamaras N, Hesley J, Chen Y-W, Funes C et al. Multiparameter in vitro assessment of compound effects on cardiomyocyte physiology using iPSC cells. J Biomol Screen 2013;18(1):39–53. https://doi.org/10.1177/1087057112457590.

[13] Abi-Gerges N, Pointon A, Oldman KL, Brown MR, Pilling MA, Sefton CE et al. Assessment of extracellular field potential and Ca2+ transient signals for early QT/pro-arrhythmia detection using human induced pluripotent stem cell-derived cardiomyocytes. J Pharmacol Toxicol Methods 2017;83:1–15. https://doi.org/10.1016/j.vascn.2016.09.001.

[14] Schild A, Bhardwaj R, Wenger N, Tscherrig D, Kandasamy P, Dernič J et al. Synthesis and Pharmacological Characterization of 2-Aminoethyl Diphenylborinate (2-APB) Derivatives for Inhibition of Store-Operated Calcium Entry (SOCE) in MDA-MB-231 Breast Cancer Cells. Int J Mol Sci 2020;21(16). https://doi.org/10.3390/ijms21165604.

[15] Rodriguez M, Beauverger P, Naime I, Rique H, Ouvry C, Souchaud S et al. Cloning and molecular characterization of the novel human melanin-concentrating hormone receptor MCH2. Mol Pharmacol 2001;60(4):632–9.

[16] Pande J, Grover AK. Plasma membrane calcium pumps in smooth muscle: from fictional molecules to novel inhibitors. Can J Physiol Pharmacol 2005;83(8-9):743–54. https://doi.org/10.1139/y05-075.

[17] Pande J, Mallhi KK, Grover AK. A novel plasma membrane Ca(2+)-pump inhibitor: caloxin 1A1. Eur J Pharmacol 2005;508(1-3):1–6. https://doi.org/10.1016/j.ejphar.2004.11.057.

[18] Pande J, Mallhi KK, Grover AK. Role of third extracellular domain of plasma membrane Ca2+-Mg2+-ATPase based on the novel inhibitor caloxin 3A1. Cell Calcium 2005;37(3):245–50. https://doi.org/10.1016/j.ceca.2004.10.004.

[19] Pande J, Mallhi KK, Sawh A, Szewczyk MM, Simpson F, Grover AK. Aortic smooth muscle and endothelial plasma membrane Ca2+ pump isoforms are inhibited differently by the extracellular inhibitor caloxin 1b1. Am J Physiol Cell Physiol 2006;290(5):C1341-9. https://doi.org/10.1152/ajpcell.00573.2005.

[20] Grover AK. Use of allosteric targets in the discovery of safer drugs. Med Princ Pract 2013;22(5):418–26. https://doi.org/10.1159/000350417.

[21] Mohamed TMA, Zakeri SA, Baudoin F, Wolf M, Oceandy D, Cartwright EJ et al. Optimisation and validation of a high throughput screening compatible assay to identify inhibitors of the plasma membrane calcium ATPase pump—a novel therapeutic target for contraception and malaria. J Pharm Pharm Sci 2013;16(2):217–30. https://doi.org/10.18433/J3PG68.

[22] Garcia IJP, Oliveira GC de, Moura Valadares JM de, Banfi FF, Andrade SN, Freitas TR et al. New bufadienolides extracted from Rhinella marina inhibit Na,K-ATPase and induce apoptosis by activating caspases 3 and 9 in human breast and ovarian cancer cells. Steroids 2019;152:108490. https://doi.org/10.1016/j.steroids.2019.108490.

[23] Kimura M, Mochizuki H, Satou R, Iwasaki M, Kokubu E, Kono K et al. Plasma Membrane Ca2+-ATPase in Rat and Human Odontoblasts Mediates Dentin Mineralization. Biomolecules 2021;11(7). https://doi.org/10.3390/biom11071010.

[24] Mishra VK, Palgunachari MN, Segrest JP, Anantharamaiah GM. Interactions of synthetic peptide analogs of the class A amphipathic helix with lipids. Evidence for the snorkel hypothesis. J Biol Chem 1994;269(10):7185–91.

[25] Hunt DJ, Jones PP, Wang R, Chen W, Bolstad J, Chen K et al. K201 (JTV519) suppresses spontaneous Ca2+ release and 3Hryanodine binding to RyR2 irrespective of FKBP12.6 association. Biochem J 2007;404(3):431–8. https://doi.org/10.1042/BJ20070135.

[26] Lock JT, Parker I, Smith IF. A comparison of fluorescent Ca^{2+} indicators for imaging local Ca^{2+} signals in cultured cells. Cell Calcium 2015;58(6):638–48. https://doi.org/10.1016/j.ceca.2015.10.003.

[27] McClenaghan C, Zeng F, Verkuyl JM. TRPA1 agonist activity of probenecid desensitizes channel responses: consequences for screening. Assay Drug Dev Technol 2012;10(6):533–41. https://doi.org/10.1089/adt.2012.447.

[28] Bartok A, Weaver D, Golenár T, Nichtova Z, Katona M, Bánsághi S et al. IP3 receptor isoforms differently regulate ER-mitochondrial contacts and local calcium transfer. Nat Commun 2019;10(1):3726. https://doi.org/10.1038/s41467-019-11646-3.

[29] Raszewski JA, Sharma S. StatPearls: Physiology, Ryanodine Receptor. Treasure Island (FL); 2021.

[30] Loncke J, Kaasik A, Bezprozvanny I, Parys JB, Kerkhofs M, Bultynck G. Balancing ER-Mitochondrial Ca2+ Fluxes in Health and Disease. Trends Cell Biol 2021;31(7):598–612. https://doi.org/10.1016/j.tcb.2021.02.003.

[31] Magi S, Piccirillo S, Preziuso A, Amoroso S, Lariccia V. Mitochondrial localization of NCXs: Balancing calcium and energy homeostasis. Cell Calcium 2020;86:102162. https://doi.org/10.1016/j.ceca.2020.102162.

[32] Dong H, Dunn J, Lytton J. Stoichiometry of the Cardiac Na+/Ca2+ exchanger NCX1.1 measured in transfected HEK cells. Biophys J 2002;82(4):1943–52. https://doi.org/10.1016/S0006-3495(02)75543-4.

[33] Yoshikawa A, van Breemen C, Isenberg G. Buffering of plasmalemmal Ca2+ current by sarcoplasmic reticulum of guinea pig urinary bladder myocytes. Am J Physiol 1996;271(3 Pt 1):C833-41. https://doi.org/10.1152/ajpcell.1996.271.3.C833.

[34] Liao Y, Erxleben C, Yildirim E, Abramowitz J, Armstrong DL, Birnbaumer L. Orai proteins interact with TRPC channels and confer responsiveness to store depletion. Proc Natl Acad Sci U S A 2007;104(11):4682–7. https://doi.org/10.1073/pnas.0611692104.

[35] Vanderkooi JM, Maniara G, Green TJ, Wilson DF. An optical method for measurement of dioxygen concentration based upon quenching of phosphorescence. J Biol Chem 1987;262(12):5476–82.

[36] Irving E, Stoker AW. Vanadium Compounds as PTP Inhibitors. Molecules 2017;22(12). https://doi.org/10.3390/molecules22122269.

[37] Fantus IG, Tsiani E. Multifunctional actions of vanadium compounds on insulin signaling pathways: evidence for preferential enhancement of metabolic versus mitogenic effects. Mol Cell Biochem 1998;182(1-2):109–19.

[38] Stankiewicz PJ, Tracey AS, Crans DC. Inhibition of phosphate-metabolizing enzymes by oxovanadium(V) complexes. Met Ions Biol Syst 1995;31:287–324.

[39] Arkin MR, Connor PR, Emkey R, Garbison KE, Heinz BA, Wiernicki TR et al. Assay Guidance Manual: FLIPR™ Assays for GPCR and Ion Channel Targets. Bethesda (MD); 2004.

[40] Boutin JA, Legros C. The five dimensions of receptor pharmacology exemplified by melatonin receptors: An opinion. Pharmacol Res Perspect 2020;8(1):e00556. https://doi.org/10.1002/prp2.556.

[41] Boutin JA, Witt-Enderby PA, Sotriffer C, Zlotos DP. Melatonin receptor ligands: A pharmaco-chemical perspective. J Pineal Res 2020;69(3):e12672. https://doi.org/10.1111/jpi.12672.

[42] Logez C, Damian M, Legros C, Dupré C, Guéry M, Mary S et al. Detergent-free Isolation of Functional G Protein-Coupled Receptors into Nanometric Lipid Particles. Biochemistry 2016;55(1):38–48. https://doi.org/10.1021/acs.biochem.5b01040.

[43] Lautié E, Russo O, Ducrot P, Boutin JA. Unraveling Plant Natural Chemical Diversity for Drug Discovery Purposes. Front Pharmacol 2020;11:397. https://doi.org/10.3389/fphar.2020.00397.

[44] Gruber CW, Muttenthaler M, Freissmuth M. Ligand-based peptide design and combinatorial peptide libraries to target G protein-coupled receptors. Curr Pharm Des 2010;16(28):3071–88. https://doi.org/10.2174/138161210793292474.

[45] Bhattacherjee A, Wallin S. Exploring Protein-Peptide Binding Specificity through Computational Peptide Screening. PLoS Comput Biol 2013;9(10):e1003277. https://doi.org/10.1371/journal.pcbi.1003277.

[46] Hussain A, Shaw PE, Hirst JD. Molecular dynamics simulations and in silico peptide ligand screening of the Elk-1 ETS domain. J Cheminform 2011;3(1):49. https://doi.org/10.1186/1758-2946-3-49.

[47] Gógl G, Törő I, Reményi A. Protein-peptide complex crystallization: a case study on the ERK2 mitogen-activated protein kinase. Acta Crystallogr D Biol Crystallogr 2013;69(Pt 3):486–9. https://doi.org/10.1107/S0907444912051062.

[48] Gordon EM, Barrett RW, Dower WJ, Fodor SP, Gallop MA. Applications of combinatorial technologies to drug discovery. 2. Combinatorial organic synthesis, library screening strategies, and future directions. J Med Chem 1994;37(10):1385–401. https://doi.org/10.1021/jm00036a001.

[49] Gallop MA, Barrett RW, Dower WJ, Fodor SP, Gordon EM. Applications of combinatorial technologies to drug discovery. 1. Background and peptide combinatorial libraries. J Med Chem 1994;37(9):1233–51. https://doi.org/10.1021/jm00035a001.

[50] Boutin JA, Jullian M, Frankiewicz L, Galibert M, Gloanec P, Le Diguarher T et al. MCH-R1 Antagonist GPS18169, a Pseudopeptide, Is a Peripheral Anti-Obesity Agent in Mice. Molecules 2021;26(5). https://doi.org/10.3390/molecules26051291.

[51] Winter J. Bacteriophage display: Peptide libraries and drug discovery. Drug Dev. Res. 1994;33(2):71–89. https://doi.org/10.1002/ddr.430330204.

[52] Wibo M, Morel N, Godfraind T. Differentiation of Ca2+ pumps linked to plasma membrane and endoplasmic reticulum in the microsomal fraction from intestinal smooth muscle. Biochimica et Biophysica Acta (BBA) - Biomembranes 1981;649(3):651–60. https://doi.org/10.1016/0005-2736(81)90170-X.

[53] Mohamed TMA, Abou-Leisa R, Baudoin F, Stafford N, Neyses L, Cartwright EJ et al. Development and characterization of a novel fluorescent indicator protein PMCA4-GCaMP2 in cardiomyocytes. J Mol Cell Cardiol 2013;63:57–68. https://doi.org/10.1016/j.yjmcc.2013.07.007.

[54] Hallick RB, Chelm BK, Gray PW, Orozco EM. Use of aurintricarboxylic acid as an inhibitor of nucleases during nucleic acid isolation. Nucleic Acids Res 1977;4(9):3055–64. https://doi.org/10.1093/nar/4.9.3055.

[55] Cho H, Lee DY, Shrestha S, Shim YS, Kim KC, Kim M-K et al. Aurintricarboxylic acid translocates across the plasma membrane, inhibits protein tyrosine phosphatase and prevents apoptosis in PC12 cells. Mol Cells 2004;18(1):46–52.

[56] Le W-D, Colom LV, Xie W, Smith RG, Alexianu M, Appel SH. Cell death induced by β-amyloid 1–40 in MES 23.5 hybrid clone: the role of nitric oxide and NMDA-gated channel activation leading to apoptosis. Brain Res 1995;686(1):49–60. https://doi.org/10.1016/0006-8993(95)00450-5.

[57] Roberts-Lewis JM, Marcy VR, Zhao Y, Vaught JL, Siman R, Lewis ME. Aurintricarboxylic acid protects hippocampal neurons from NMDA- and ischemia-induced toxicity in vivo. J Neurochem 1993;61(1):378–81. https://doi.org/10.1111/j.1471-4159.1993.tb03583.x.

[58] Aronica EM, Gorter JA, Grooms S, Kessler JA, Bennett MV, Zukin RS et al. Aurintricarboxylic acid prevents GLUR2 mRNA down-regulation and delayed neurodegeneration in hippocampal CA1 neurons of gerbil after global ischemia. Proc Natl Acad Sci U S A 1998;95(12):7115–20. https://doi.org/10.1073/pnas.95.12.7115.

[59] Posner A, Raser KJ, Hajimohammadreza I, Yuen PW, Wang KK. Aurintricarboxylic acid is an inhibitor of mu- and m-calpain. Biochem Mol Biol Int 1995;36(2):291–9.

[60] Lewis S, Little R, Baudoin F, Prehar S, Neyses L, Cartwright EJ et al. Acute inhibition of PMCA4, but not global ablation, reduces blood pressure and arterial contractility via a nNOS-dependent mechanism. J Cell Mol Med 2018;22(2):861–72. https://doi.org/10.1111/jcmm.13371.

[61] Boutin JA, Tartar AL, van Dorsselaer A, Vaudry H. General lack of structural characterization of chemically synthesized long peptides. Protein Sci 2019;28(5):857–67. https://doi.org/10.1002/pro.3601.

[62] Pierry C, Couve-Bonnaire S, Guilhaudis L, Neveu C, Marotte A, Lefranc B et al. Fluorinated pseudopeptide analogues of the neuropeptide 26RFa: synthesis, biological, and structural studies. Chembiochem 2013;14(13):1620–33. https://doi.org/10.1002/cbic.201300325.

983 **Table 1a**: Chemical data for a first series of caloxin-derived peptides.

Code	Sequence			Rt [a] (min)	Purity (%)	MW exp.	MW theo.
cal1a1	H-	ACPWWSPHACGGG [b]	$-NH_2$	3.34	97.90	1325.60	1325.49
cal1a2	H-	ACPIWQPHYCGGG [b]	$-NH_2$	3.16	95.10	1385.50	1385.99
cal1b1	H-	TAWSEVLHLLSRGGG	$-NH_2$	1.64	96.80	1581.20	1581.80
cal1b11	H-	TAWSEVLHLLSR	$-NH_2$	5.71	95.88	1410.08	1410.62
cal1b12	H-	TAWSEVLHLLSR**X6** [c]	$-NH_2$	5.81	95.44	1523.64	1523.78
cal1b13	H-	TA**X7**SEVLHLLSRGGG	$-NH_2$	5.84	95.83	1592.64	1592.80
cal1b14	H-	TA**X16**SEVLHLLSRGGG	$-NH_2$	5.58	96.34	1599.58	1599.80
cal1b15	Ac-	TAWSEVLHLLSRGGG	$-NH_2$	5.61	95.20	1624.01	1623.80
cal1b16	H-	**X9**AWSEVLHLLSRGGG	$-NH_2$	5.49	95.44	1563.69	1563.80
cal1b3	H-	TIPKWISIIQALRGGGSK	$-NH_2$	3.75	95.01	1924.38	1924.33
cal1b31	H-	TIPKWISIIQALRGGGS	$-NH_2$	8.54	96.45	1796.07	1796.13
cal1b310	H-	ISIIQALRGGGSK	$-NH_2$	7.61	95.71	1298.63	1298.54
cal1b311	H-	TIPKWISIIQAL	$-NH_2$	2.82	95.21	1381.42	1381.70
cal1b312	H-	TIPKWISIIQA	$-NH_2$	2.39	95.57	1268.90	1268.54
cal1b313	H-	TIPKWISIIQ	$-NH_2$	2.37	95.27	1197.01	1197.47
cal1b314	H-	IPKWISIIQALR	$-NH_2$	2.58	96.04	1436.50	1436.80
cal1b315	H-	PKWISIIQALR	$-NH_2$	2.42	96.94	1323.20	1323.63
cal1b316	H-	KWISIIQALR	$-NH_2$	2.32	95.69	1226.10	1226.51
cal1b317	H-	TIPKWISIIAALR	$-NH_2$	4.20	95.01	1480.82	1480.84
cal1b318	H-	TIPKWIAIIQALR	$-NH_2$	2.64	95.00	1521.10	1521.89
cal1b319	H-	TIPKAISIIQALR	$-NH_2$	2.32	95.5	1422.63	1422.76
cal1b32	H-	TIPKWISIIQALRGGG	$-NH_2$	8.59	96.49	1709.04	1709.06
cal1b320	H-	TIPAWISIIQALR	$-NH_2$	2.96	95.17	1480.40	1480.79
cal1b321	H-	TIPKWIAIIAALRG	$-NH_2$	4.33	97.01	1521.10	1521.90

cal1b322	H-	TIPKWIAIIAALR	-NH_2	4.38	96.04	1464.50	1464.85
cal1b323	H-	TIPKWIAIIQAL	-NH_2	4.64	95.71	1365.01	1365.71
cal1b324	H-	TIPKWIAIIQA	-NH_2	4.04	97.49	1252.40	1252.55
cal1b325	H-	TIPKWIAIIQ	-NH_2	4.03	95.03	1181.38	1181.48
cal1b326	H-	TIPKWIAIIQALR	-OH	4.24	97.28	1522.08	1522.88
cal1b327	H-	**X1**IPKWIAIIAALR	-NH_2	4.30	96.95	1448.93	1448.90
cal1b328	H-	TIP**X2**WIAIIAALR	-NH_2	4.16	95.90	1422.75	1422.79
cal1b329	H-	TIPKYIAIIAALR	-NH_2	3.90	95.01	1441.31	1441.82
cal1b33	H-	TIPKWISIIQALRGG	-NH_2	8.71	96.35	1651.44	1652.01
cal1b330	H-	TIPK**X3**IAIIAALR	-NH_2	3.29	95.53	1426.51	1426.82
cal1b331	H-	CTIPKWIAIIAALRC	-NH_2	4.41	96.11	1668.98	1669.13
cal1b332		TIPKWIAIIAALRG [d]		4.91	97.05	1505.04	1504.89
cal1b333	H-	TIPKW**X4**LR	-NH_2	3.73	97.49	1095.72	1095.50
cal1b334	H-	TIPKW**X1X1X1**R	-NH_2	2.66	96.7	1054.90	1054.30
cal1b336	H-	TIpKWIAIIAALR	-NH_2	4.13	95.85	1464.59	1464.85
cal1b337	H-	TIPKWAIAALR	-NH_2	3.46	98.03	1238.00	1238.53
cal1b34	H-	TIPKWISIIQALRG	-NH_2	8.72	95.81	1594.99	1594.95
cal1b340	H-	KWIAIIAALR	-NH_2	3.77	98.73	1153.20	1153.47
cal1b341	H-	TIPKWIGIIGALR	-NH_2	3.95	96.23	1436.86	1436.79
cal1b342	H-	KWALR	-NH_2	2.45	97.33	671.67	671.84
cal1b343/cal1d1 [e]	H-	KW**X5**LR	-NH_2	3.51	98.48	798.17	798.09
cal1b35	H-	TIPKWISIIQALR	-NH_2	8.79	96.38	1537.86	1537.90
cal1b36	H-	IPKWISIIQALRGGGSK	-NH_2	8.25	97.28	1823.12	1823.20
cal1b37	H-	PKWISIIQALRGGGSK	-NH_2	8.05	95.3	1710.09	1710.04
cal1b38	H-	KWISIIQALRGGGSK	-NH_2	7.93	96.63	1612.44	1612.93
cal1b39	H-	WISIIQALRGGGSK	-NH_2	8.36	95.43	1484.71	1484.75
cal1c2	H-	TAWSEVLDLLRRGGGSK	-NH_2	3.67	97.02	1843.69	1843.11

cal2a1	H-	VSNSNWPSFPSSGGG	-NH_2	3.20	95.06	1478.20	1478.54
cal3a1	H-	WSSTSSVSAPLFGGGGSAK	-NH_2	4.51	95.57	1782.01	1781.95
cal3a2	H-	DSHINNEPSRRKGGGK	-NH_2	1.56	95.16	1750.33	1750.90

[a] Retention time determined by by HPLC or by UPLC.

[b] Disulfide-bridged peptides.

[c] **X1**: γ-amino-butyric acid; **X2**: 2,3-diamino-propionic acid; **X3**: 3-(4-pyridyl)-Ala-OH; **X4**: 11-amino-undecanoic acid; **X5**: 12-amino-dodecanoic acid; **X6**: 6-amino-hexanoic acid; **X7**: H-Ala(2-naphtyl)-OH; **X9**: (*S*)-azetidine-2-carboxylic acid; **X16**: β-(2-benzothiazolyl)-Ala-OH. Fmoc-derivatives are reported in Table 2.

[d] Head-to-tail cyclopeptide.

[e] **Cal1b343** was renamed **cal1d1** (see below, **Table 1b**).

992
993 **Table 1b**: Chemical data for caloxin1d1-derived peptides.

Code	Sequence			Rt [a] (min)	Purity (%)	MW exp.	MW theo.
cal1d1	H-	KW**X5**LR [b]	$-NH_2$	3.51	98.48	798.17	798.09
cal1d11	H-	KW**X4**LR	$-NH_2$	3.47	98.84	784.28	784.06
cal1d12	H-	KW**X10**LR	$-NH_2$	3.03	99.29	742.50	741.98
cal1d13	H-	KW**X11**LR	$-NH_2$	2.62	97.64	700.00	699.90
cal1d14	H-	KWIAILR	$-NH_2$	3.15	95.43	898.40	898.15
cal1d15	H-	KWAILR	$-NH_2$	2.85	96.82	785.20	784.99
cal1d16	H-	KWIIIIIILR	$-NH_2$	4.55	90.02	1279.40	1279.71
cal1d17	H-	KWAAAAAALR	$-NH_2$	2.83	95.97	1027.01	1027.23
cal1d18	H-	**X12**WIAIIAALR	$-NH_2$	3.76	95.18	1139.02	1139.50
cal1d19	H-	**X13**WIAIIAALR	$-NH_2$	3.80	95.73	1125.66	1125.41
cal1d20	H-	**X2**WIAIIAALR	$-NH_2$	3.88	95.38	1111.98	1111.38
cal1d21	H-	KWIAIIAALA	$-NH_2$	4.35	97.94	1068.40	1068.36
cal1d22	H-	KWIAIIAALK	$-NH_2$	3.84	97.31	1125.74	1125.45
cal1d23	H-	rlaaiiaiwk [c,d]	$-NH_2$	3.62	95.18	1153.72	1153.47
cal1d25	H-	K**X8**IAIIAALR	$-NH_2$	4.00	97.26	1171.00	1170.50
cal1d26	H-	K**X14**IAIIAALR	$-NH_2$	3.23	98.68	1154.46	1154.40
cal1d27	H-	KH**X5**LR	$-NH_2$	2.82	95.54	750.00	749.10
cal1d28	H-	**X2**W**X5**LR	$-NH_2$	3.66	98.91	755.79	755.99
cal1d29	H-	**X13**W**X5**LR	$-NH_2$	3.62	97.55	769.74	770.02
cal1d30	H-	**X12**W**X5**LR	$-NH_2$	3.62	98.01	783.72	784.10
cal1d31	H-	KW**X5**L**X21**	$-NH_2$	3.65	98.95	811.86	812.10
cal1d32	H-	KW**X11X11**LR	$-NH_2$	3.49	97.49	798.56	799.02
cal1d33	H-	KW**X11X11X11**LR	$-NH_2$	3.46	96.84	898.08	898.15
cal1d34	H-	KW**X11X11X11X11**LR	$-NH_2$	2.83	96.22	996.62	997.30

cal1d35	H-	KWGGGGGGLR	-NH_2	2.17	98.02	942.60	943.07
cal1d36	H-	KW**X10X10**LR	-NH_2	3.37	99.01	883.10	883.20
cal1d37	H-	KW**X15**LR	-NH_2	2.73	98.18	803.40	804.01
cal1d38	H-	KW**X19**LR	-NH_2	2.82	97.53	847.40	848.06
cal1d39	H-	KW**X19**R	-NH_2	2.31	96.49	734.04	734.90
cal1d40	H-	KW**X17X17**R	-NH_2	3.37	98.30	741.32	741.97
cal1d41	H-	**X12**HIAIIAALR	-NH_2	2.88	98.94	1089.72	1090.20
cal1d42	H-	kW**X5**LR [d]	-NH_2	4.33	98.22	797.58	798.07
cal1d43	H-	K**X18X5**LR	-NH_2	3.69	98.14	811.58	812.10
cal1d44	H-	KF**X5**LR	-NH_2	4.29	97.38	758.54	759.04
cal1d45	H-	KY**X5**LR	-NH_2	3.99	99.79	774.48	775.04
cal1d46	H-	K**X7X5**LR	-NH_2	3.87	99.06	808.50	809.10
cal1d47	H-	KW**X20**LR	-NH_2	4.08	99.68	839.61	840.17
cal1d48	H-	KW**X20**R	-NH_2	3.66	98.96	726.32	727.01
cal1d49	H-	**X12**W**X5**L**X21**	-NH_2	3.55	99.10	797.18	798.09
cal1d50	H-	KW**X22**LR	-NH_2	3.48	96.79	795.55	796.07
cal1d51	Ac-	KW**X5**LR	-NH_2	3.94	98.71	839.60	840.13
cal1d52	H-	**X9**W**X5**LR	-NH_2	3.94	96.78	752.80	753.01
cal1d53	H-	**X23**W**X5**LR	-NH_2	4.22	99.62	782.41	783.08
cal1d54	H-	K(**X5**RL)W [e]	-NH_2	3.32	97.79	797.90	798.09
cal1d55	H-	KW**X5**LR	-OH	3.59	98.95	798.60	799.07
cal1d56	H-	KW**X5**L**X24**	-NH_2	3.85	98.17	798.70	799.07
cal1d57	H-	**X9**KW**X5**LR	-NH_2	3.58	95.25	880.80	881.18
cal1d58	H-	KW**X5**L**X25**	-NH_2	3.53	98.93	825.80	826.14
cal1d59	H-	KW**X5**L**X26**	-NH_2	3.93	99.15	842.70	843.09
cal1d60	H-	K**X23X5**LR	-NH_2	3.76	99.33	814.50	815.14
cal1d61	H-	K**X14X5**LR [f]	-NH_2	2.85	97.05	798.90	799.08

cal1d62		H-	K**X14X5**LR [f]	-NH_2	3.02	95.05	799.10	799.08
cal1d63		H-	KW**X27**LR	-NH_2	3.67	95.08	824.26	824.13
cal1d64		H-	KW**X28**LR	-NH_2	3.19	97.74	793.64	794.06
cal1d65		H-	KW**X29**LR	-NH_2	3.29	97.69	815.94	816.12
cal1d66		H-	KW**X30**LR	-NH_2	3.09	95.36	799.62	800.06
cal1d67		H-	KW**X31**LR	-NH_2	2.63	98.83	822.80	823.06
cal1d68		H-	KW	-NH_2	1.69	98.79	331.50	331.42
cal1d69		Ac-	LR	-NH_2	2.11	97.94	328.80	328.22
cal1d70		H-	KW + LR [g]	-NH_2	same as above			
cal1d71a		H-	KW**X32**LR [h]	-NH_2	3.79	95.49	837.60	838.16
cal1d71b		H-	KW**X32**LR [h]	-NH_2	3.81	96.69	837.60	838.16
cal1d72		H-	KW**X33**LR	-NH_2	3.45	99.26	832.14	832.11
cal1d73		H-	KW**X34**LR	-NH_2	3.63	99.49	812.57	812.12
cal1d74		Ac-	TIPKWIA**X35**AALR	-NH_2	3.72	94.44	1396.88	1397.02
cal1d76		H-	GW**X5**LR	-NH_2	3.98	95.13	726.88	726.97
cal1d77		H-	AW**X5**LR	-NH_2	3.84	96.81	740.84	741.00
cal1d78		H-	**X23**W**X5**LR	-NH_2	4.12	97.45	782.94	783.08
cal1d79		H-	RL**X5**WK [i]	-NH_2	3.58	90.47	797.58	798.10
cal1d80		H-	rl**X5**wk [d,j]	-NH_2	3.49	98.82	798.10	798.09
cal1d81 [k]	(*SR*)	H-	**X12X14X5X26**	-NH_2	3.15	95.65	829.90	830.10
	(*RS*)				3.15	95.65		
cal1d82		H-	EW**X5**LR	-NH_2	3.83	97.47	799.00	799.10
cal1d83		H-	**X36**W**X5**LR	-NH_2	3.90	97.86	826.92	827.08
cal1d84		H-	**X37**W**X5**LR	-NH_2	3.95	97.49	840.54	840.11
cal1d85		H-	**X6**W**X5**LR	-NH_2	3.91	98.03	782.70	783.08
cal1d86		H-	KW**X5**AR	-NH_2	3.08	95.15	755.98	756.10
cal1d87		H-	KW**X5**IR	-NH_2	3.44	97.21	798.00	798.10

cal1d88	H-	KW**X5X23**R	-NH_2	3.61	96.91	798.00	798.10
cal1d89	H-	KW**X5X38**R	-NH_2	3.23	95.08	802.00	802.10

[a] Retention time determined by by HPLC or by UPLC.

[b] **X2**: 2,3-diamino-propionic acid; **X4**: 11-amino-undecanoic acid; **X5**: 12-amino-dodecanoic acid; **X6**: 6-amino-hexanoic acid; **X7**: H-Ala(2-naphtyl)-OH; **X8**: β-(3-benzothienyl)-Ala-OH; **X9**: (*S*)-azetidine-2-carboxylic acid; **X10**: 8-amino-octanoic acid; **X11**: 5-amino-pentanoic acid; **X12**: ornithine; **X13**: 2,4-diamino-butyric acid; **X14**: (DL)-7-azatryptophan; **X15**: 12-amino-4,7,10-trioxa-dodecanoic acid; **X17**: 7-amino-heptanoic acid; **X18**: H-Trp(Me)-OH; **X19**: 15-amino-4,7,10,13-tetraoxa-pentadecanoic acid; **X20**: 15-amino-pentadecanoic acid; **X21**: H-homoArg-OH; **X22**: 12-amino-dode-7-enoic acid; **X23**: H-Nle-OH; **X24**: H-Cit-OH; **X25**: H-Arg(*N*ω,*N*ω-dimethyl)-OH; **X26**: H-Arg(NO_2)-OH; **X27**: 14-amino-tetradec-2-enoic acid; **X28**: 11-amino-undec-8-ynoic acid; **X29**: 9-(aminomethylsulfanyl)nonanoic acid; **X30**: 3-(7-aminoheptoxy)propanoic acid; **X31**: 4-[1-(5-aminopentyl)triazol-4-yl]butanoic acid; **X32**: 3-[4-(6-aminohexyl)cyclohexyl]propanoic acid; **X33**: 3-[4-(6-aminohexyl)phenyl]propanoic acid; **X34**: 12-amino-8-methyl-dodecanoic acid; **X35**: 3,4-diamino-benzoic acid; **X36**: 2-amino-heptane-1,7-dioic acid; **X37**: 2-amino-octane-1,8-dioic acid; **X38**: H-homoCys-OH. Fmoc-derivatives are reported in Table 2.

[c] Retro-inverso version of **cal1b340**.

[d] Lowercase letters indicate D-amino acid.

[e] The "**X5**RL-" moiety is branched onto the ε-NH_2 of the lysine residue.

[f] **X14** was used as racemate. Diastereoisomers (**cal1d61** and **cal1d62**) were separated and purified independently. No enantiomeric identification was performed.

[g] Equimolar mixture of the two dipeptides.

[h] **X32** was used as racemate. Diastereoisomers (**cal1d71a** and **cal1d71b**) were separated and purified independently. No enantiomeric identification was performed.

[i] Retro version of **cal1d1**.

[j] Retro-inverso version of **cal1d1**.

[k] **X14** was used as racemate, but as opposed to precedingly ([f]), the diastereoisomers were not separated and purified, but the mixture was tested as such.

1021

1022 **Table 2**: Non-standard Fmoc-amino acid building blocks.

Residue X code	Building block name	Residue name	CAS number
X1	Fmoc-γ-amino-butyric acid	Abu	116821-47-7
X2	*N*α-Fmoc-*N*β-alloc-L-2,3-diamino-propionic acid	Dap	188970-92-5
X3	Fmoc-3-(4-pyridyl)-Ala-OH	Pal	169555-93-5
X4	Fmoc-11-amino-undecanoic acid	Aun	88574-07-6
X5	Fmoc-12-amino-dodecanoic acid	Ado	128917-74-8
X6	Fmoc-6-amino-hexanoic acid	Ahx	88574-06-5
X7	Fmoc-3-(2-naphtyl)-Ala-OH	Nal	112883-43-9
X8	Fmoc-β-(3-benzothienyl)-Ala-OH	Bta	177966-60-8
X9	1-Fmoc-(*S*)-azetidine-2-carboxylic acid	Aze	136552-06-2
X10	Fmoc-8-amino-octanoic acid	Aoc	126631-93-4
X11	Fmoc-5-amino-pentanoic acid	Ava	123622-48-0
X12	*N*α-Fmoc- *N*δ-Boc-ornithine	Orn	109425-55-0
X13	*N*α-Fmoc-*N*γ-Boc-L-2,4-diamino-butyric acid	Dab	125238-99-5
X14	Fmoc-(DL)-7-azatryptophan	-	7146-37-4 [a]
X15	Fmoc-12-amino-4,7,10-trioxa-dodecanoic acid	-	867062-95-1
X16	Fmoc-β-(2-benzothiazolyl)-Ala-OH	-	959583-56-3
X17	Fmoc-7-amino-heptanoic acid	-	127582-76-7
X18	Fmoc-Trp(Me)-OH	Trp(Me)	1334509-86-2
X19	Fmoc-15-amino-4,7,10,13-tetraoxa-pentadecanoic acid	-	557756-85-1
X20	Fmoc-15-amino-pentadecanoic acid	-	17437-21-7 [a]
X21	Fmoc-homoArg(Pbf)-OH	*h*Arg	401915-53-5
X22	Fmoc-12-amino-dode-7-enoic acid	-	N/A
X23	Fmoc-Nle-OH	Nle	77284-32-3
X24	Fmoc-Cit-OH	Cit	133174-15-9
X25	*N*α-Fmoc-*N*ω,*N*ω-dimethyl-Arg(Pbf)-OH	ADMA	11858411-84-2
X26	Fmoc-Arg(NO_2)-OH	Arg(NO_2)	58111-94-7

X27	Fmoc-14-amino-tetradec-2-enoic acid	-	[b]
X28	Fmoc-11-amino-undec-8-ynoic acid	-	N/A
X29	Fmoc-9-(aminomethylsulfanyl)nonanoic acid	-	N/A
X30	Fmoc-3-(7-aminoheptoxy)propanoic acid	-	[b]
X31	Fmoc-4-[1-(5-aminopentyl)triazol-4-yl]butanoic acid	-	N/A
X32	Fmoc-3-[4-(6-aminohexyl)cyclohexyl]propanoic acid	-	[b]
X33	Fmoc-3-[4-(6-aminohexyl)phenyl]propanoic acid	-	[b]
X34	Fmoc-12-amino-8-methyl-dodecanoic acid	-	N/A
X35	Fmoc-3-amino-Boc-4-amino-benzoic acid	Dbz	1823479-63-5
X36	Fmoc-2-amino-heptanedioic acid-7-tert-butyl ester	-	159751-46-9
X37	Fmoc-2-amino-octanedioic acid-8-tert-butyl ester	Asu	276869-41-1
X38	Fmoc-homoCys(Trt)-OH	*h*Cys	167015-23-8

[a]The CAS number belongs to the unprotected derivative. Fmoc protecting group was introduced as previously described [62].

[b] Compounds custom-synthesized for the Institut de Recherches Servier.

N/A, not applicable.

1029 **Table 3**: Sequences and Ki of reference caloxins.

Code	Sequence			PMCA1 Ki (μM) [a]	PMCA2 Ki (μM) [a]
cal1a1	H-	ACPWWSPHACGGG [b]	$-NH_2$		500
cal1a2	H-	ACPIWQPHYCGGG [b]	$-NH_2$		190
cal1b1	H-	TAWSEVLHLLSRGGG	$-NH_2$	100	46
cal1b3	H-	TIPKWISIIQALRGGGSK	$-NH_2$	17	45
cal1c2	H-	TAWSEVLDLLRRGGGSK	$-NH_2$	21	2
cal2a1	H-	VSNSNWPSFPSSGGG	$-NH_2$		500
cal3a1	H-	WSSTSSVSAPLFGGGGSAK	$-NH_2$		700
cal3a2	H-	DSHINNEPSRRKGGGK	$-NH_2$		86

1030 [a] Adapted from Grover et al., [20].
1031 [b] Disulfide-bridged peptides.
1032
1033

Table 4: First series of caloxin 1b1 analogues.

Code	Sequence		
cal1b1	H-	TAWSEVLHLLSRGGG	-NH_2
cal1b11	H-	TAWSEVLHLLSR	-NH_2
cal1b12	H-	TAWSEVLHLLSR**X6** [a]	-NH_2
cal1b13	H-	TA**X7**SEVLHLLSRGGG	-NH_2
cal1b14	H-	TA**X16**SEVLHLLSRGGG	-NH_2
cal1b15	Ac-	TAWSEVLHLLSRGGG	-NH_2
ca1b16	H-	**X9**AWSEVLHLLSRGGG	-NH_2

[a] **X6**: 6-amino-hexanoic acid; **X7**: H-Ala(2-naphtyl)-OH; **X9**: (*S*)-azetidine-2-carboxylic acid; **X16**: H-Ala(2-benzothiazolyl)-OH. Fmoc-derivatives are reported in Table 2.

1042 **Table 5**: Sequence alignments of caloxin 1b3 downsized analogues.

Code	Sequence		
cal1b3	H-	TIPKWISIIQALRGGGSK	-NH_2
cal1b31	H-	TIPKWISIIQALRGGGS	-NH_2
cal1b32	H-	TIPKWISIIQALRGGG	-NH_2
cal1b33	H-	TIPKWISIIQALRGG	-NH_2
cal1b34	H-	TIPKWISIIQALRG	-NH_2
cal1b35	H-	TIPKWISIIQALR	-NH_2
cal1b311	H-	TIPKWISIIQAL	-NH_2
cal1b312	H-	TIPKWISIIQA	-NH_2
cal1b313	H-	TIPKWISIIQ	-NH_2
cal1b36	H-	IPKWISIIQALRGGGSK	-NH_2
cal1b37	H-	PKWISIIQALRGGGSK	-NH_2
cal1b38	H-	KWISIIQALRGGGSK	-NH_2
cal1b39	H-	WISIIQALRGGGSK	-NH_2
cal1b310	H-	ISIIQALRGGGSK	-NH_2
cal1b314	H-	IPKWISIIQALR	-NH_2
cal1b315	H-	PKWISIIQALR	-NH_2
cal1b316	H-	KWISIIQALR	-NH_2

1043

Table 6: Point-substituted analogues of **cal1b35**.

Code	Sequence		
cal1b35	H-	TIPKWISIIQALR	-NH_2
cal1b317	H-	TIPKWISIIAALR [a]	-NH_2
cal1b318	H-	TIPKWIAIIQALR	-NH_2
cal1b319	H-	TIPKAISIIQALR	-NH_2
cal1b320	H-	TIPAWISIIQALR	-NH_2
cal1b321	H-	TIPKWIAIIAALRG	-NH_2
cal1b322	H-	TIPKWIAIIAALR	-NH_2
cal1b323	H-	TIPKWIAIIQAL	-NH_2
cal1b324	H-	TIPKWIAIIQA	-NH_2
cal1b325	H-	TIPKWIAIIQ	-NH_2
cal1b326	H-	TIPKWIAIIQALR	-OH
cal1b327	H-	**X1**IPKWIAIIAALR [b]	-NH_2
cal1b328	H-	TIP**X2**WIAIIAALR	-NH_2
cal1b329	H-	TIPKYIAIIAALR	-NH_2
cal1b330	H-	TIPK**X3**IAIIAALR	-NH_2
cal1b331	H-	CTIPKWIAIIAALRC [c]	-NH_2
cal1b333	H-	TIPKW**X**4LR	-NH_2
cal1b334	H-	TIPKW**X1X1X1**R	-NH_2
cal1b336	H-	TIpKWIAIIAALR [d]	-NH_2
cal1b337	H-	TIPKWAIAALR	-NH_2
cal1b340	H-	KWIAIIAALR	-NH_2
cal1b341	H-	TIPKWIGIIGALR	-NH_2
cal1b332		TIPKWIAIIAALRG [e]	
cal1b342	H-	KWALR	-NH_2
cal1d19	H-	**X13**WIAIIAALR	-NH_2

[a] Red letters denote ala-scan position.

[b] **X1**: γ-amino-butyric acid; **X2**: 2,3-diamino-propionic acid; **X3**: H-Ala(4-pyridyl)-OH; **X4**: 11-amino-undecanoic acid; **X13**: 2,4-diamino-butyric acid. Fmoc-derivatives are reported in Table 2.

[c] Disulfide-bridged peptide.

[d] Lowercase letters indicate D-amino acid.

[e] Head-to-tail cyclopeptide.

1055 **Table 7**: First series of caloxin **1b340** analogues.

Code	Sequence			ΔAUC (30 μM) [a]
cal1b340	H-	KWIAIIAALR	$-NH_2$	615.7 ± 49.3
cal1d19	H-	**X13**WIAIIAALR [b]	$-NH_2$	452.2 ± 27.1
cal1d20	H-	**X2**WIAIIAALR	$-NH_2$	339.8 ± 23.8
cal1d25	H-	K**X16**IAIIAALR	$-NH_2$	414.7 ± 24.9
cal1d26	H-	K**X14**IAIIAALR	$-NH_2$	0.0 ± 0.0
cal1d21	H-	KWIAIIAALA	$-NH_2$	88.3 ± 7.9
cal1d22	H-	KWIAIIAALK	$-NH_2$	377.9 ± 41.6
cal1d23	H-	kwiaiiaalr [c]	$-NH_2$	49.0 ± 1.0

1056 [a] The higher the ΔAUC, the more potent the inhibition.
1057 [b] **X2**: 2,3-diamino-propionic acid; **X13**: 2,4-diamino-butyric acid; **X14**: (DL)-7-azatryptophan;
1058 **X16**: H-Ala(2-benzothiazolyl)-OH. Fmoc-derivatives are reported in Table 2.
1059 [c] Retro-inverso version of **cal1b340**.
1060

1061

1062

Table 8: Chemical data and PMCA inhibiting activities of centrally modified caloxin1d (**cal1b340**) analogues.

Code	N-ter	Sequence of the heavy atoms in the central region	C-ter	Number of heavy atoms in the central region	ΔAUC (30 µM) [a]	Chemical name of the spacer
cal1b340	KW-	$(N\text{-}C\text{-}CO)_6$	-LR-NH_2	18	615.7 ± 55.4	-Ile-Ala-$(Ile)_2$-$(Ala)_2$-
cal1d68		0	-LR-NH_2	N/A	0.8 ± 0.0	N/A
cal1d69	KW-	0	-NH_2	N/A	5.2 ± 0.5	N/A
cal1d70	KW-	0	-LR-NH_2	N/A	4.2 ± 0.3	N/A
cal1b342	KW-	N-C-CO	-LR-NH_2	3	0.0 ± 0.0	-Ala-
cal1d13	KW-	N-C_4-CO	-LR-NH_2	6	0.0 ± 0.0	-**X11**-, 5-amino-pentanoic acid
cal1d15	KW-	$(N\text{-}C\text{-}CO)_2$	-LR-NH_2	6	0.0 ± 0.0	-Ala-Ile-
cal1d14	KW-	$(N\text{-}C\text{-}CO)_3$	-LR-NH_2	9	0.0 ± 0.0	-Ile-Ala-Ile-
cal1d12	KW-	N-C_7-CO	-LR-NH_2	9	0.0 ± 0.0	-**X10**-, 8-amino-octanoic acid
cal1d11	KW-	N-C_{10}-CO	-LR-NH_2	12	0.0 ± 0.0	-**X4**-, 11-amino-undecanoic acid
cal1d32	KW-	$(N\text{-}C_4\text{-}CO)_2$	-LR-NH_2	12	0.0 ± 0.0	-**X11**-, 5-amino-pentanoic acid
cal1d66	KW-	N-C_7-O-C_2-CO	-LR-NH_2	12	0.0 ± 0.0	-**X30**-, 3-(7-aminoheptoxy)propanoic acid
cal1d37	KW-	$(O\text{-}C_2)_3$	-LR-NH_2	12	133.6 ± 8.0	-**X15**-, 12-amino-4,7,10-trioxa-dodecanoic acid
cal1d64	KW-	N-C_2-C≡C-C_6-CO	-LR-NH_2	12	125.7 ± 12.6	-**X28**-, 11-amino-undec-8-ynoic acid
cal1d39	KW-	$(O\text{-}C_2)_4$	-R-NH_2	12	128.1 ± 7.7	-**X19**-, 15-amino-4,7,10,13-tetraoxa-pentadecanoic acid
cal1d1 (cal1b343)	KW-	N-C_{11}-CO	-LR-NH_2	13	572.7 ± 40.1	-**X5**-, 12-amino-dodecanoic acid
cal1d65	KW-	N-C-S-C_8-CO	-LR-NH_2	12	72.9 ± 5.1	-**X29**-, 9-(aminomethylsulfanyl)nonanoic acid
cal1d50	KW-	N-C_4-C=C-C_5-CO	-LR-NH_2	13	239.5 ± 19.2	-**X22**-, 12-amino-dode-7-enoic acid
cal1d63	KW-	N-C_{11}-C=C-CO	-LR-NH_2	15	519.7 ± 46.8	-**X27**-, 14-amino-tetradec-2-enoic acid
cal1d38	KW-	$(O\text{-}C_2)_4$	-LR-NH_2	12	170.1 ± 8.5	-**X19**-, 15-amino-4,7,10,13-tetraoxa-pentadecanoic acid
cal1d40	KW-	$(N\text{-}C_6\text{-}CO)_2$	-LR-NH_2	16	167.4 ± 6.7	-**X17**-, 7-amino-heptanoic acid
cal1d47	KW-	N-C_{14}-CO	-LR-NH_2	16	116.6 ± 10.5	-**X20**-, 15-amino-pentadecanoic acid
cal1d48	KW-	N-C_{14}-CO	-R-NH_2	16	166.3 ± 18.3	-**X20**-, 15-amino-pentadecanoic acid
cal1d16	KW-	$(N\text{-}C\text{-}CO)_6$	-LR-NH_2	18	0.0 ± 0.0	-$(Ile)_6$-

cal1d17	KW-	$(N\text{-}C\text{-}CO)_6$	-LR-NH_2	18	0.0 ± 0.0	$\text{-(Ala)}_6\text{-}$
cal1d33	KW-	$(N\text{-}C_4\text{-}CO)_3$	-LR-NH_2	18	0.0 ± 0.0	-**X11**-, 5-amino-pentanoic acid
cal1d35	KW-	$(N\text{-}C\text{-}CO)_6$	-LR-NH_2	18	0.0 ± 0.0	$\text{-(Gly)}_6\text{-}$
cal1d36	KW-	$(N\text{-}C_7\text{-}CO)_2$	-LR-NH_2	18	10.3 ± 0.6	-**X10**-, 8-amino-octanoic acid
cal1d34	KW-	$(N\text{-}C_4\text{-}CO)_4$	-LR-NH_2	24	0.0 ± 0.0	-**X11**-, 5-amino-pentanoic acid

[a] The higher the ΔAUC, the more potent the inhibition.

N/A: not applicable.

1068 **Table 9**: Chemical data and PMCA inhibiting activities of other centrally modified caloxin1d (**cal1b340**) analogues.

Code	N-ter	Sequence of the heavy atoms in the central region	C-ter	Number of heavy atoms in the central region	ΔAUC (30 µM) [a]	Chemical name of the spacer
cal1d67	KW-	N-C_5-triazole-C_3-CO	-LR-NH_2	13	0.0 ± 0.0	-**X31**-, 4-[1-(5-aminopentyl)triazol-4-yl]butanoic acid
cal1d72	KW-	N-C_6-phenyl-C_2-CO	-LR-NH_2	14	710.1 ± 63.8	-**X33**-, 3-[4-(6-aminohexyl)phenyl]propanoic acid
cal1d71	KW-	N-C_6-cyclohexyl-C_2-CO	-LR-NH_2	14	846.3 ± 59.2	-**X32**-, 3-[4-(6-aminohexyl)cyclohexyl]propanoic acid
cal1d73	KW-	N-C_4-C(CH_3)-C_6-CO	-LR-NH_2	13	902.4 ± 126.4	-**X34**-, 12-amino-8-methyl-dodecanoic acid

1069 [a] The higher the ΔAUC, the more potent the inhibition.
1070
1071
1072
1073
1074
1075

Table 10: Chemical data and PMCA inhibiting activities of N-terminal modified **cal1d1** analogues.

Code	Sequence			ΔAUC (30 μM) [a]
cal1d1	H-	KW**X5**LR [b]	-NH_2	572.7 ± 39.2
cal1d41	H-	**X12**HIAIIAALR	-NH_2	169.5 ± 17.4
cal1d18	H-	**X12**WIAIIAALR	-NH_2	443.0 ± 27.1
cal1d55	H-	KW**X5**LR	-OH	120.7 ± 10.0
cal1d51	Ac-	KW**X5**LR	-NH_2	4.5 ± 0.0
cal1d42	H-	kW**X5**LR	-NH_2	694.6 ± 83.3
cal1d76	H-	GW**X5**LR	-NH_2	645.5 ± 45.4
cal1d77	H-	AW**X5**LR	-NH_2	524.4 ± 47.1
cal1d83	H-	**X36**W**X5**LR	-NH_2	331.4 ± 33.2
cal1d84	H-	**X37**W**X5**LR	-NH_2	309.2 ± 36.8
cal1d85	H-	**X6**W**X5**LR	-NH_2	286.6 ± 32.2
cal1d78	H-	**X23**W**X5**LR	-NH_2	775.4 ± 101.4
cal1d82	H-	EW**X5**LR	-NH_2	275.6 ± 18.9
cal1d28	H-	**X2**W**X5**LR	-NH_2	874.6 ± 61.2
cal1d29	H-	**X13**W**X5**LR	-NH_2	495.1 ± 39.7
cal1d30	H-	**X12**W**X5**LR	-NH_2	688.8 ± 62.1
cal1d49	H-	**X12**W**X5**L**X21**	-NH_2	701.6 ± 69.8
cal1d53	H-	**X23**W**X5**LR	-NH_2	635.2 ± 69.6
cal1d57	H-	**X9**KW**X5**LR	-NH_2	255.7 ± 33.4
cal1d52	H-	**X9**W**X5**LR	-NH_2	292.9 ± 22.9
cal1d43	H-	K**X18X5**LR	-NH_2	765.2 ± 60.7
cal1d44	H-	KF**X5**LR	-NH_2	362.8 ± 25.0
cal1d45	H-	KY**X5**LR	-NH_2	241.8 ± 10.3
cal1d27	H-	KH**X5**LR	-NH_2	10.0 ± 0.0
cal1d46	H-	K**X7X5**LR	-NH_2	620.7 ± 62.1
cal1d60	H-	K**X23X5**LR	-NH_2	326.7 ± 22.8
cal1d61	H-	K**X14X5**LR [c]	-NH_2	224.2 ± 20.2
cal1d62	H-	K**X14X5**LR [c]	-NH_2	402.6 ± 35.9

[a] The higher the ΔAUC, the more potent the inhibition.

[b] **X2**: 2,3-diamino-propionic acid; **X5**: 12-amino-dodecanoic acid; **X6**: 6-amino-hexanoic acid; **X7**: H-Ala(2-naphtyl)-OH; **X9**: (*S*)-azetidine-2-carboxylic acid; **X12**: ornithine; **X13**: 2,4-diamino-butyric acid; **X14**: (DL)-7-azatryptophan; **X18**: H-Trp(Me)-OH; **X21**: H-homoArg-OH; **X23**: H-Nle-OH; **X36**: 2-amino-heptane-1,7-dioic acid; **X37**: 2-amino-octane-1,8-dioic acid. Fmoc-derivatives are reported in Table 2.

[c] **X14** was used as racemate. Diastereoisomers (**cal1d61** and **cal1d62**) were separated and purified independently. No enantiomeric identification was performed.

Table 11: Chemical data and PMCA inhibiting activities of C-terminal modified **cal1d1** analogues.

Code	Sequence			ΔAUC (30 μM) [a]
cal1d1	H-	KW**X5**LR [b]	$-NH_2$	572.7 ± 39.2
cal1d86	H-	KW**X5**AR	$-NH_2$	298.9 ± 20.8
cal1d87	H-	KW**X5**IR	$-NH_2$	851.5 ± 76.7
cal1d88	H-	KW**X5X23**R	$-NH_2$	830.7 ± 91.3
cal1d89	H-	KW**X5X38**R	$-NH_2$	855.5 ± 111.1
cal1d31	H-	KW**X5**L**X21**	$-NH_2$	344.1 ± 10.4
cal1d56	H-	KW**X5**L**X24**	$-NH_2$	11.7 ± 1.1
cal1d58	H-	KW**X5**L**X25**	$-NH_2$	116.6 ± 5.9

[a] The higher the ΔAUC, the more potent the inhibition

[b] **X5**: 12-amino-dodecanoic acid; **X21**: H-homoArg-OH; **X23**: H-Nle-OH; **X24**: H-Cit-OH; **X25**: H-Arg(*N*ω,*N*ω-dimethyl)-OH; **X38**: H-homoCys-OH. Fmoc-derivatives are reported in Table 2.

Table 12: Summary, apparent potencies of the 12 best peptides.

Code	Sequence			Ratio to cal1d1	Ratio to cal1b3	Potency [a]
cal1b3	H-	TIPKWISIIQALRGGGSK	-NH_2		1.0	
cal1d1	H-	KW**X5**LR [b]	-NH_2	1.0	1.6	
cal1d80	H-	rl**X5**wk [c,d]	-NH_2	2.1	3.5	
cal1d49	H-	**X12**W**X5X21**	-NH_2	2.1	4.3	
cal1d53	H-	**X23**W**X5**LR	-NH_2	1.9	3.9	
cal1d71a	H-	KW**X32**LR [e]	-NH_2	1.9	3.1	
cal1d79	H-	RL**X5**WK	-NH_2	1.9	3.1	
cal1d73	H-	KW**X34**R	-NH_2	1.9	3.0	
cal1d89	H-	KW**X5X38**R	-NH_2	1.8	2.9	
cal1d87	H-	KW**X5**IR	-NH_2	1.8	2.9	
cal1d71b	H-	KW**X32**LR [e]	-NH_2	1.8	2.8	
cal1d88	H-	KW**X5X23**R	-NH_2	1.7	2.8	
cal1d28	H-	**X2**W**X5**LR	-NH_2	1.5	3.9	
cal1d72	H-	KW**X33**LR	-NH_2	1.5	2.4	
cal1d43	H-	K**X18X5**LR	-NH_2	1.3	3.4	
cal1d42	H-	kW**X5**LR	-NH_2	1.2	3.1	
cal1d30	H-	**X12**W**X5**LR	-NH_2	1.2	3.0	
cal1d46	H-	K**X7X5**LR	-NH_2	1.1	2.7	

[a] Red, apparent IC_{50} around 30 µM; yellow: apparent IC_{50} around 10 µM; green: apparent IC_{50} around 5 µM.

[b] **X2**: 2,3-diamino-propionic acid; **X5**: 12-amino-dodecanoic acid; **X7**: H-Ala(2-naphtyl)-OH; **X12**: ornithine; **X18**: H-Trp(Me)-OH; **X21**: H-homoArg-OH; **X23**: H-Nle-OH; **X32**: 3-[4-(6-aminohexyl)cyclohexyl]propanoic acid; **X33**: 3-[4-(6-aminohexyl)phenyl]propanoic acid; **X34**: 12-amino-8-methyl-dodecanoic acid; **X38**: H-homoCys-OH. Fmoc-derivatives are reported in Table 2.

[c] Lowercase letters indicate D-amino acid.

[d] Retro-inverso version of **cal1d1**.

[e] **X32** was used as racemate. Diastereoisomers (**cal1d71a** and **cal1d71b**) were separated and purified independently. No enantiomeric identification was performed.

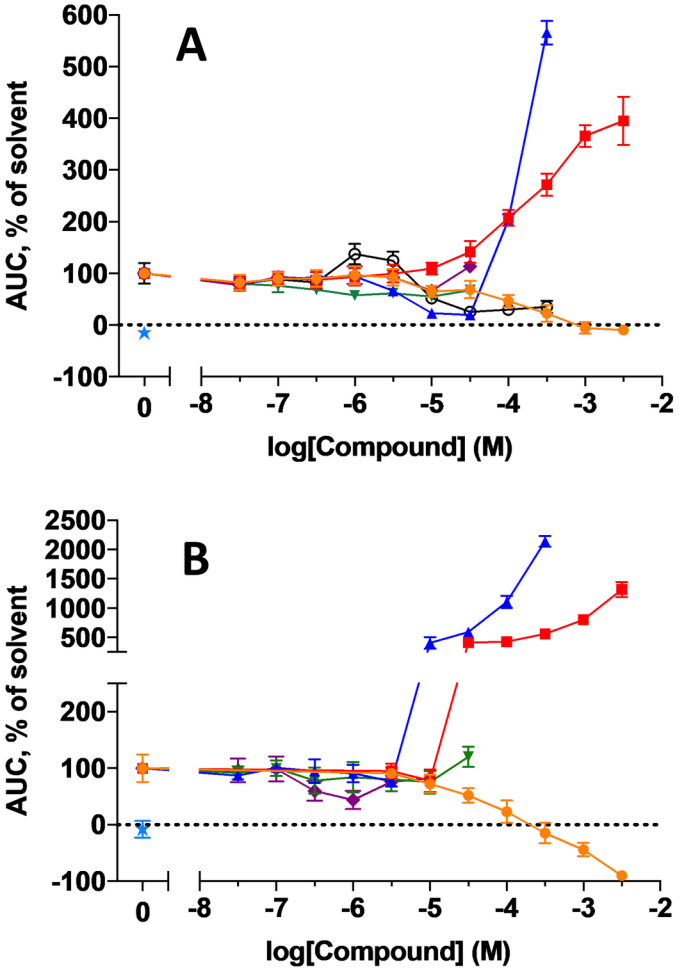
A
AUC, % of solvent
600
500
400
300
200
100
0
-100
0
-8
-7
-6
-5
-4
-3
-2
log[Compound] (M)
B
AUC, % of solvent
2500
2000
1500
1000
500
200
100
0
-100
0
-8
-7
-6
-5
-4
-3
-2
log[Compound] (M)

Figure 1

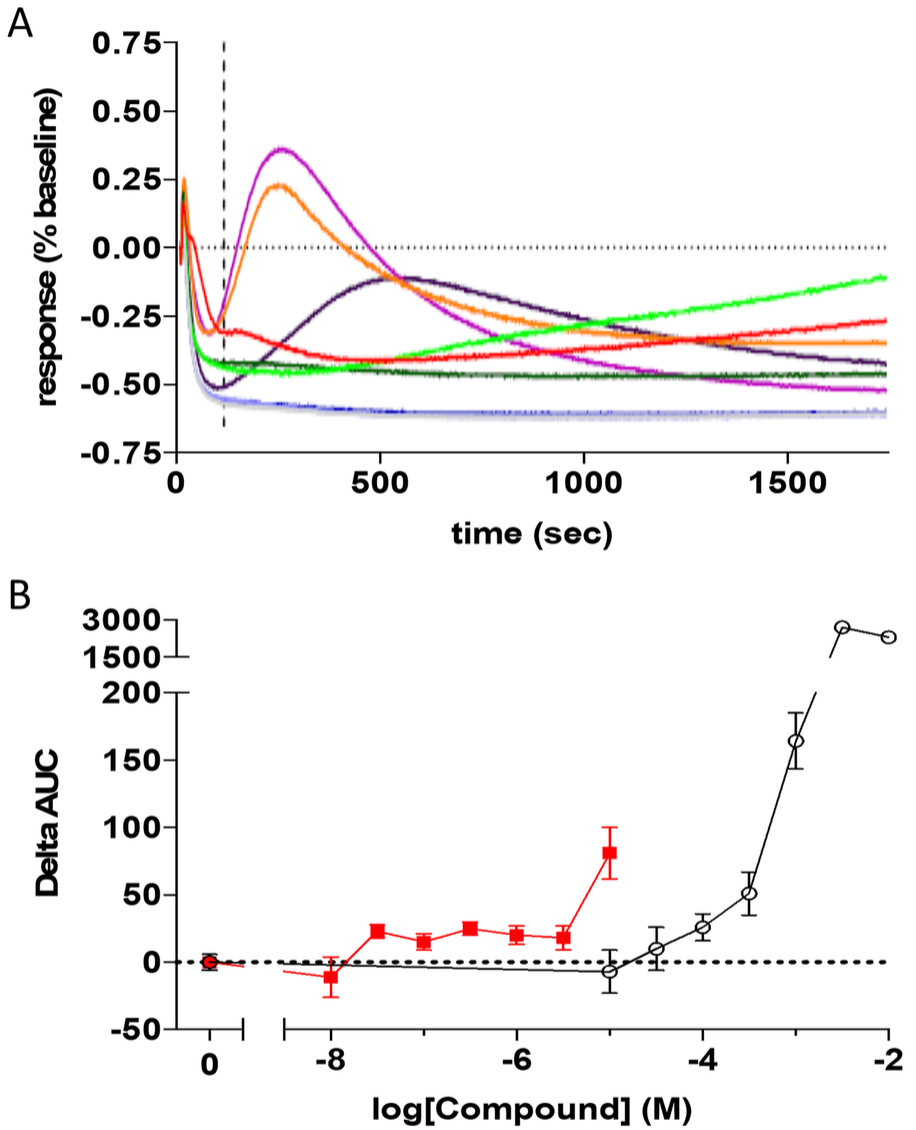
A
0.75
0.50
0.25
0.00
-0.25
-0.50
-0.75
response (% baseline)
0
500
1000
1500
time (sec)
B
3000
1500
200
150
100
50
0
-50
Delta AUC
0
-8
-6
-4
-2
log[Compound] (M)

Figure 2

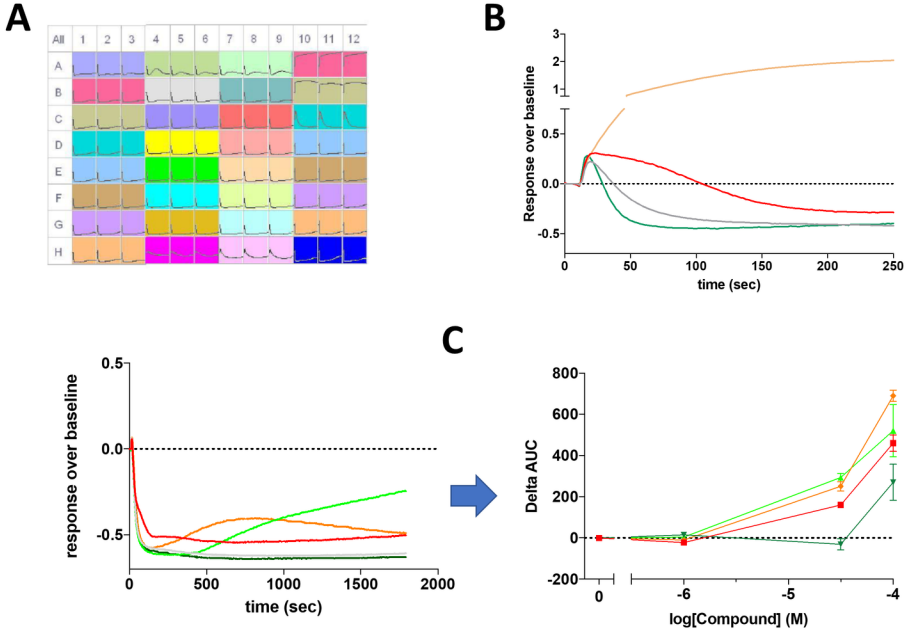
A
All 1 2 3 4 5 6 7 8 9 10 11 12
A
B
C
D
E
F
G
H
B
Response over baseline
3
2
1
0.5
0.0
-0.5
0
50
100
150
200
250
time (sec)
C
response over baseline
0.5
0.0
-0.5
0
500
1000
1500
2000
time (sec)
Delta AUC
800
600
400
200
0
-200
0
-6
-5
-4
log[Compound] (M)

Figure 3

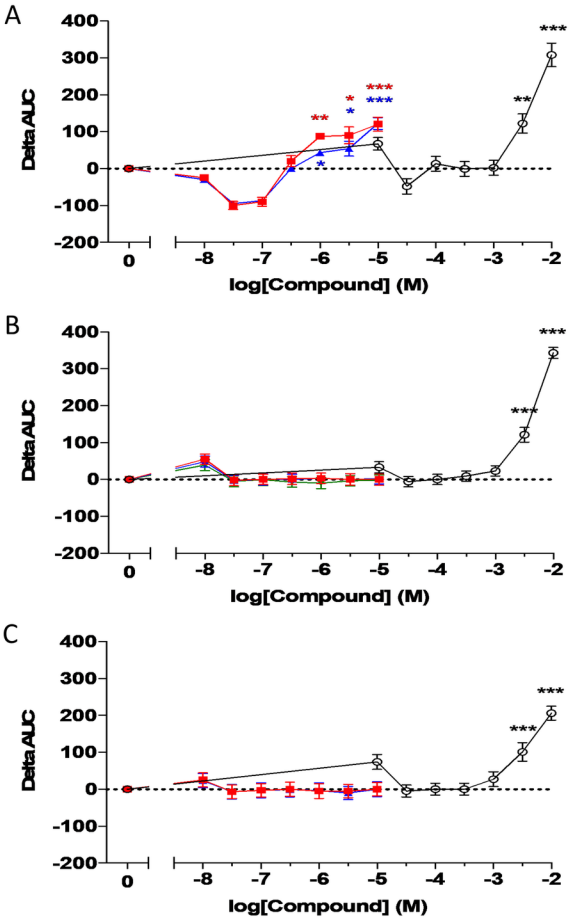
A
B
C
Delta AUC
400
300
200
100
0
-100
-200
0
-8
-7
-6
-5
-4
-3
-2
log[Compound] (M)
*
**
***

Figure 4

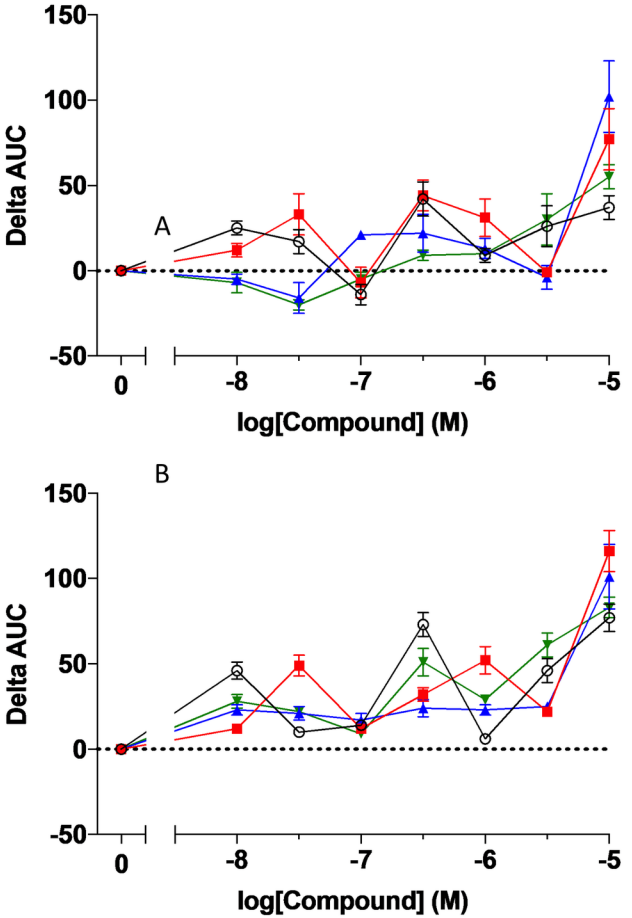

Figure 5

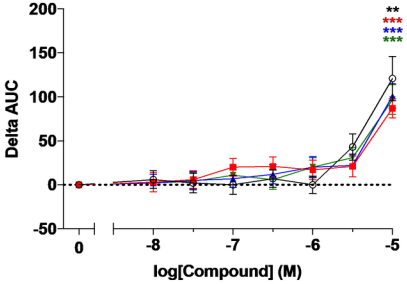
Delta AUC
200
150
100
50
0
-50
0
-8
-7
-6
-5
log[Compound] (M)
**
***
***
***

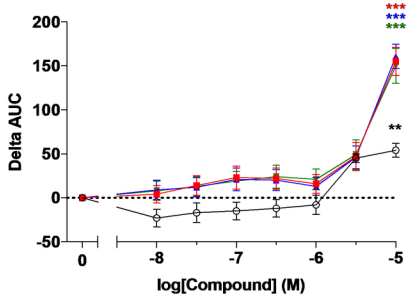
Delta AUC
200
150
100
50
0
-50
0
-8
-7
-6
-5
log[Compound] (M)
***
***
***
**

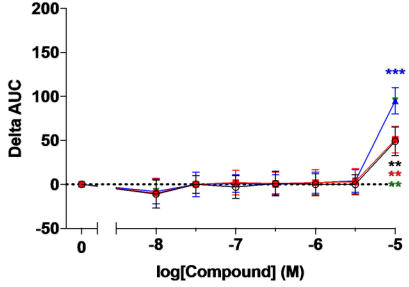
Delta AUC
200
150
100
50
0
-50
0
-8
-7
-6
-5
log[Compound] (M)
***
**
**
***

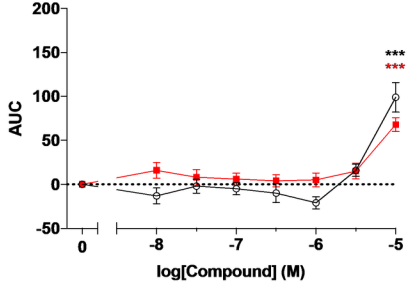
AUC
200
150
100
50
0
-50
0
-8
-7
-6
-5
log[Compound] (M)
***
***

Figure 6

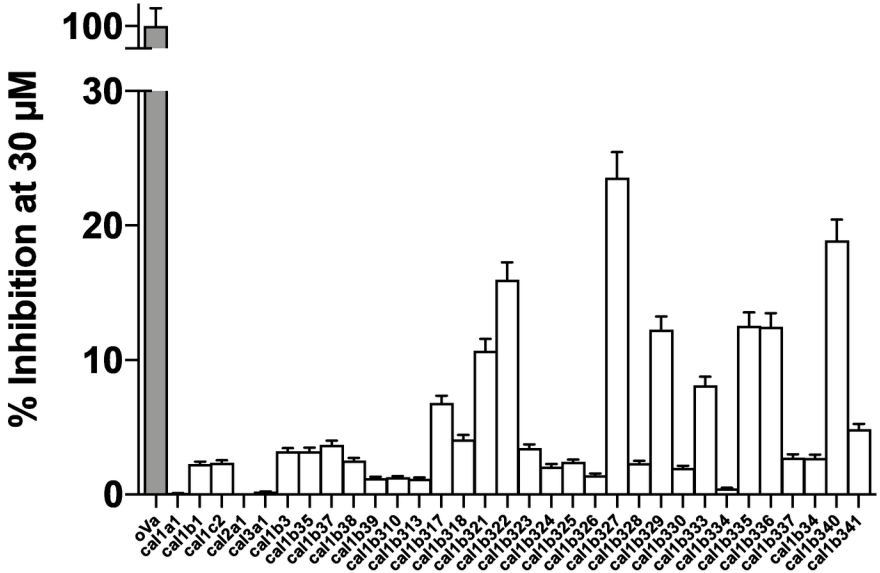
% Inhibition at 30 µM
100
30
20
10
0
oVa
cal1a1
cal1b1
cal1c2
cal2a1
cal3a1
cal1b3
cal1b35
cal1b37
cal1b38
cal1b39
cal1b310
cal1b313
cal1b317
cal1b318
cal1b321
cal1b322
cal1b323
cal1b324
cal1b325
cal1b326
cal1b327
cal1b328
cal1b329
cal1b330
cal1b333
cal1b334
cal1b335
cal1b336
cal1b337
cal1b34
cal1b340
cal1b341

Figure 7

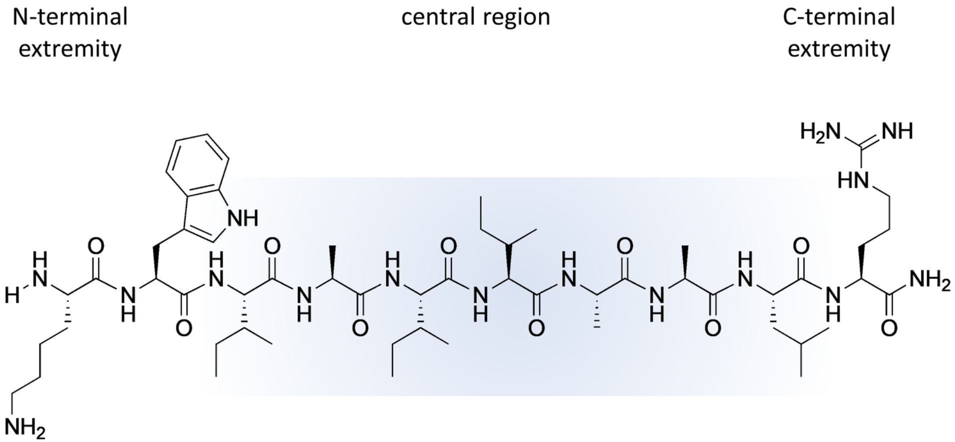
N-terminal extremity
central region
C-terminal extremity
NH
H_2N
NH
HN
NH_2
NH_2

Figure 8

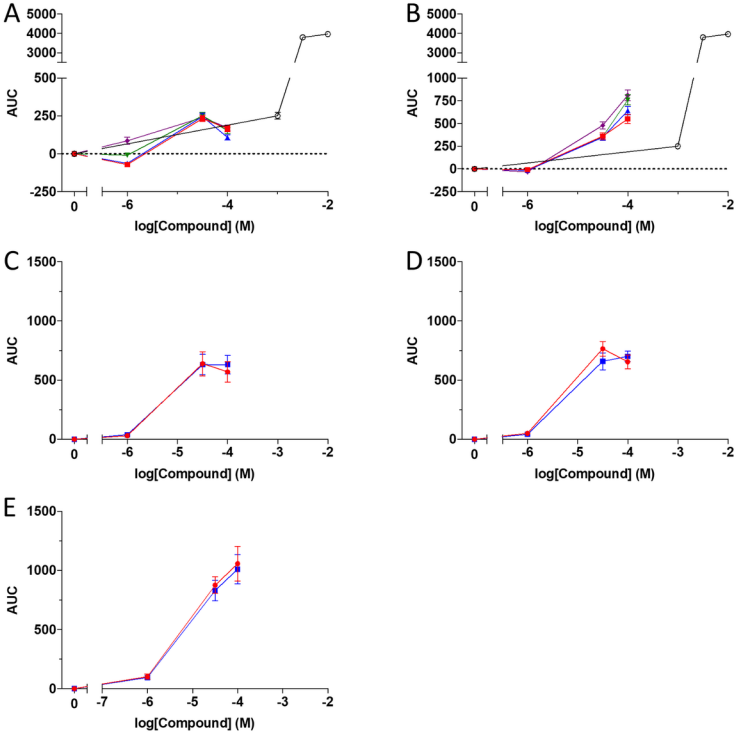

Figure 9